Fokker–Planck model for computational studies of monatomic rarefied gas flows

M. H. GORJI[1]†, M. TORRILHON[2] AND P. JENNY[1]

[1]Institute of Fluid Dynamics, ETH Zentrum, Sonneggstrasse 3, 8092 Zürich, Switzerland
[2]Department of Mathematics, RWTH Aachen University, Schinkestrasse 2, D-52062 Aachen, Germany

In this study, we propose a non-linear continuous stochastic velocity process for simulations of monatomic gas flows. The model equation is derived from a Fokker–Planck approximation of the Boltzmann equation. By introducing a cubic non-linear drift term, the model leads to the correct Prandtl number of 2/3 for monatomic gas, which is crucial to study heat transport phenomena. Moreover, a highly accurate scheme to evolve the computational particles in velocity- and physical space is devised. An important property of this integration scheme is that it ensures energy conservation and honours the tortuosity of particle trajectories. Especially in situations with small to moderate Knudsen numbers, this allows to proceed with much larger time steps than with direct simulation Monte Carlo (DSMC), i.e. the mean collision time not necessarily has to be resolved, and thus leads to more efficient simulations. Another computational advantage is that no direct collisions have to be calculated in the proposed algorithm. For validation, different micro-channel flow test cases in the near continuum and transitional regimes were considered. Detailed comparisons with DSMC for Knudsen numbers between 0.07 and 2 reveal that the new solution algorithm based on the Fokker–Planck approximation for the collision operator can accurately predict molecular stresses and heat flux and thus also gas velocity and temperature profiles. Moreover, for the Knudsen Paradox, it is shown that good agreement with DSMC is achieved up to a Knudsen number of about 5.

Key words: Computational methods, kinetic theory, non-continuum effects

1. Introduction

It is widely known that the Navier–Stokes equations, in the original form, cannot properly account for gas flows where the mean free path length λ of the molecules is not insignificantly small compared to the characteristic length L of the problem. In such situations, with Knudsen numbers $Kn = \lambda/L$ larger than approximately 0.01, non-equilibrium effects become important and boundary conditions have to be modified. There exist many different areas with relevant applications where $Kn \gtrsim 0.01$, e.g. micro-electro-mechanical systems (MEMS) or aerospace vehicles in a rarefied atmosphere, and thus there is a significant interest in efficient and accurate simulation models for this kind of flows. The Boltzmann equation can successfully describe the dynamics of gas flows in non-continuum flow regimes. However, due to the complexity of the collision operator and the high dimensionality of the equation (three spatial

† Email address for correspondence: gorjih@ifd.mavt.ethz.ch

plus three velocity dimensions plus time), its direct numerical solution is extremely costly and for most applications infeasible. Therefore, various approximations of the Boltzmann equation that are more computationally attractive have been introduced. Most of all, DSMC is often used as a reference for other models (Bird 1994). In DSMC, representative binary collisions are performed consistent with the collision operator. However, even though simplifications are involved, DSMC still can become computationally very expensive. Especially, if the Knudsen number is not very large, one is forced to compute a huge number of collisions. Another problem is related to the statistical noise, especially if the Mach number is very low. Nevertheless, DSMC has proven, to be very accurate for rarefied gas flow simulations and thus will be regarded as a benchmark reference in the following discussion of further approximations. However, it is to be emphasized that modelling issues related to the boundary condition or polyatomic molecules are still under development for DSMC. On the other hand, continuum equations like the system of compressible gas dynamics or moment equations can be viewed as models for Boltzmann equations, which are computationally very efficient. The statistical description of the flow is represented by a finite number of velocity moments, for which partial differential equations (in physical space and time) have to be solved. For example, in the R13 moment equations, the evolution of mass density, velocity, molecular stresses and heat fluxes for the gas is solved (see Struchtrup 2005; Torrilhon & Struchtrup 2008). In this context, also Euler or Navier–Stokes equations are moment-based models, which can be extended by higher order approximations such as Burnett or super-Burnett equations. For computational efficiency of these moment methods, see Zheng, Resse & Struchtrup (2006). Although accurate results for certain flow scenarios up to moderate Kn can be achieved in normal shock waves (see e.g. Agarwal, Yun & Balakrishnan 2001; Torrilhon & Struchtrup 2004) or channel flows in the slip regime (see e.g. Beskok & Karniadakis 1999), in all moment equations one has to deal with unclosed fluxes, i.e. higher moments, that have to be modelled. Part of this closure problem arises due to transport, as well as due to the correct treatment of the collision integral. Another class of models is based on an approximation of the collision operator, e.g. the famous BGK model (Bhatnagar, Gross & Krook 1954) which has been extensively studied in various works (see e.g. Cercignani 1988; Sharipov & Seleznev 1998). Usually, such model equations are derived from Boltzmann based on the assumption that the molecular velocity distribution is not too far from equilibrium. Compared to moment equations, these are equations in the higher dimensional physical-velocity space (like the Boltzmann equation) and therefore more expensive to solve; however, they are applicable in a wider range of Knudsen numbers. Extensions have been made based on the BGK kinetic model which successfully provide correct Pr of 2/3 for monatomic molecules, e.g. ES-BGK (Holway 1966) or S-Model (Shakhov 1968) to name a few. The Fokker–Planck description as a model equation for gas dynamics has been discussed by various authors (see Lebowitz, Frisch & Helfand 1960; Pawula 1967; Cercignani 1988; Heinz 2004; Yano, Suzuki & Kuroda 2009; Jenny, Torrilhon & Heinz 2010). While Pawula (1967) and Lebowitz *et al.* (1960) tried to approximate the Boltzmann equation by a Fokker–Planck equation, their simple drift models result in a wrong Prandtl number Pr for monatomic gas molecules. More recently, Heinz (2004) introduced an acceleration model with an additional time scale, which can be used to adjust the Prandtl number. However, the physical interpretation of such an acceleration model is not clear. Yano *et al.* (2009) proposed a Fokker–Planck equation with a source term to correct Pr. Later, Jenny *et al.* (2010) introduced a stochastic solution algorithm based on the Fokker–Planck approximation for simulations of

rarefied gas flows. Very good agreement of molecular stresses and mean velocity in comparison with DSMC, linearized Boltzmann and experiment has been achieved. Heat fluxes and temperature, however, are in disagreement as expected due to wrong Pr. An important advantage of this solution algorithm is its computational efficiency, since it allows the employment of a time integration scheme which does not require to resolve the collisions. In comparison with BGK-based models which describe jump-type stochastic processes for evolution of the molecular velocity distribution, the proposed solution algorithm, on the other hand, employs a diffusion-type process, whereas much larger time steps and coarser spatial discretization become possible. The current paper is an extension of the work by Jenny *et al.* (2010) with the objective to fix the problem with the wrong Prandtl number. This was achieved by introducing a drift term which is nonlinear with respect to the molecular velocity. Numerical validation studies with Knudsen numbers up to 5 confirm that first, second and third velocity moments are in excellent agreement with DSMC. Moreover, the efficient particle integration scheme could be generalized for the non-linear particle evolution. The paper is structured as follows. In §2, the new Fokker–Planck equation with a cubic (in velocity) drift coefficient is introduced. Section 3 deals with the numerical algorithm to solve the corresponding Langevin equation; its detailed derivation is shown in the Appendix. Numerical studies including homogeneous relaxation of the molecular velocity distribution and various micro-channel gas flow test cases are presented in §4 and compared with DSMC. Finally, §5 contains some concluding remarks.

2. Fokker–Planck approximation of the kinetic theory

The non-continuum flow regimes are associated with situations where the macroscopic properties of the flow are not only functions of themselves but depend also on the microscopic details. On the other hand, for practical problems, it is computationally impossible to treat each microscopic interaction. Therefore, the kinetic theory based on statistical mechanics was introduced to study non-continuum gas flows.

2.1. *Basic equations*

For a statistical description of gas flow, the molecular chaos assumption is adopted. To better understand, let us consider the physical-velocity space with the coordinates $\boldsymbol{x}$ and $\boldsymbol{V}$, respectively. In the kinetic theory, the mechanical state of monatomic gas is fully determined by the positions $\boldsymbol{X}^\alpha(t)$ and velocities $\boldsymbol{M}^\alpha(t)$ of all encompassed molecules α, which is represented by the molecular density function $\mathscr{F}(\boldsymbol{x}, \boldsymbol{V}, t)$. The evolution of $\mathscr{F}$, for simple monatomic gas molecules, is governed by the Boltzmann equation

$$\frac{\partial \mathscr{F}}{\partial t} + V_i \frac{\partial \mathscr{F}}{\partial x_i} + G_i \frac{\partial \mathscr{F}}{\partial V_i} = -\frac{1}{\rho} \int_{\mathbb{R}^3} \int_0^{4\pi} \sigma |\boldsymbol{V} - \boldsymbol{V}'| \mathscr{F}(\boldsymbol{V}) \mathscr{F}(\boldsymbol{V}') \, \mathrm{d}\Omega \, \mathrm{d}\boldsymbol{V}'$$
$$+ \frac{1}{\rho} \int_{\mathbb{R}^3} \int_0^{4\pi} \sigma |\boldsymbol{V} - \boldsymbol{V}'| \mathscr{F}(\boldsymbol{V}^c) \mathscr{F}(\boldsymbol{V}'^c) \, \mathrm{d}\Omega \, \mathrm{d}\boldsymbol{V}' \quad (2.1)$$

where $\rho(\boldsymbol{x}, t) = \int_{\mathbb{R}^3} \mathscr{F}(\boldsymbol{x}, \boldsymbol{V}, t) \, \mathrm{d}\boldsymbol{V}$ is the gas density and $\boldsymbol{G}$ an external force, which is considered to be independent of the molecular velocities. Note that here, like in the following, Einstein's summation convention is used. The first right-hand-side (r.h.s.) term describes the rate at which molecules with velocity $\boldsymbol{V}$ collide with others (only binary collisions are considered), which depends on the relative particle velocity and

the total collision cross section $\int_0^{4\pi} \sigma \, d\Omega$. The second rhs term on the other hand describes at which rate molecules adopt velocity V due to collisions, where (V^c, V'^c) are the deterministic post-collision velocities as functions of the pre-collision state (V, V') and the post-collision relative velocity angle Ω.

From now on, we refer to the rhs of (2.1) as the Boltzmann collision operator $S^{Boltz}(\mathscr{F})$.

Note that the mass density function $\mathscr{F}$ is related to the probability density function (PDF) f as $\mathscr{F}(V, x, t) = \rho(x, t) f(V; x, t)$. The high dimensionality of the space in which $\mathscr{F}$ evolves together with the complexity of the collision operator makes direct numerical solutions of the Boltzmann equation extremely expensive and thus this approach is limited to few simple problems. Therefore, computationally more attractive approximations of S^{Boltz} are in high demand. Some of them are mentioned in the Introduction and here only the Fokker–Planck approximation is further discussed.

2.2. *Fokker–Planck approximation*

It has been shown by others that a Fokker–Planck (FP) approximation of the Boltzmann collision operator can be used up to quite large Knudsen numbers and that it in terms of computational cost it is much more attractive than DSMC (Jenny *et al.* 2010). Here, we generalize the simple linear model with the objective to fix inconsistencies regarding the Prandtl number. Therefore, the generalized form

$$S^{FP} = -\frac{\partial(A_i \mathscr{F})}{\partial V_i} + \frac{D^2}{2} \frac{\partial^2 \mathscr{F}}{\partial V_j \partial V_j} \tag{2.2}$$

is considered with the drift and diffusion coefficients $A_i(v', x, t)$ and $D(x, t)$, respectively. Those are functions of the peculiar velocity $v' = V - U$, where the mean (or gas) velocity is defined as $U = \int_{\mathbb{R}^3} V f \, dV$. The goal is to construct the rhs of (2.2) such that $\mathscr{F}$ relaxes towards a Maxwellian distribution like in other models as e.g. BGK. To study related aspects and assumptions, first the relevant modelling issues and then physical interpretations are discussed.

2.2.1. *Modelling aspects*

Some basic properties of S^{FP}, which are a requirement for any physically acceptable collision model, e.g. Galilean invariance, conservation of mass, momentum and energy have already been shown by Jenny *et al.* (2010). Moreover, the H-theorem and accordingly the second law of thermodynamics can be proved for the Fokker–Planck equation with A_i being time-independent (see Shiino 1987). However, here as we are considering a more general ansatz for A_i, hence the proof of the H-theorem becomes more challenging. Nevertheless, studying the evolution of the Boltzmann H-function and consequently the H-theorem using the generalized FP equation, i.e. (2.2) is beyond the scope of this paper.

Here, we point out some additional features of the FP operator, which makes it attractive as an approximation of the Boltzmann collision term. For example, relaxation of higher order moments can be controlled by appropriate expressions of A_i as polynomial functions of V_i. This leads to a set of macroscopic moment equations, which are consistent with the Boltzmann equation in the Chapman–Enskog approximation with physically correct macroscopic coefficients like viscosity μ and the Prandtl number Pr. We will apply this procedure with a cubic polynomial ansatz for the drift coefficient. Moreover, we point out that as the FP approximation is a model equation for the molecular velocity distribution function, therefore no closure problem exists. At the same time, one can convert the FP model to an equivalent

Langevin-type stochastic differential equation (SDE). In this context, many particles have to be evolved in a manner similar to that in DSMC; however, since the Langevin-type SDEs describe continuous velocity processes and no direct particle collisions have to be considered, highly efficient numerical integration schemes can be developed allowing for much larger time steps. It is important to mention that the simulated particles do not represent real molecules; they have to be regarded as computational particles employed to solve the corresponding FP equation.

2.2.2. *Physical interpretation*

The physical assumptions implied by the FP model are that the particle velocities change due to a permanent stochastic force and not due to discrete collisions. Particle interaction thus occurs due to coupling through the coefficients in the evolution equations, which are functions of stochastic moments of the local ensemble. Considering the extreme case of infinite Knudsen number, i.e. no inter-molecular collisions occur, S^{FP} as well as S^{Boltz} become zero and thus the FP and DSMC models become identical. In the other extreme case of extremely small Knudsen numbers, the Navier–Stokes equations are recovered by both the FP model and DSMC; the only concern here is consistency of the macroscopic coefficients. More challenging to model is the intermediate Knudsen number range, which is important for many relevant applications and here it is investigated to which extent the FP model suggested in this paper is applicable.

2.2.3. *Drift coefficients*

Drift and diffusion coefficients A_i and D can be derived from known velocity moment evolutions as described next. Here, relaxation of moments up to the heat flux is derived from the Boltzmann equation assuming Maxwellian molecules. Note, however, that higher moments could also be included leading to not only more general, but also more complicated models. First, the velocity moments in the kinetic framework are defined. Let

$$p_{ij} = \int_{\mathbb{R}^3} v'_i v'_j \mathscr{F} \, \mathrm{d}V \tag{2.3}$$

be the pressure tensor and

$$q_i = \frac{1}{2} \int_{\mathbb{R}^3} v'_i v'_j v'_j \mathscr{F} \, \mathrm{d}V \tag{2.4}$$

the heat flux. For further derivations, the deviatoric part of a tensor p_{ij} will be denoted as $p_{\langle ij \rangle} = (1/2)(p_{ij} + p_{ji}) - (1/3)p_{kk}\delta_{ij}$, where δ_{ij} is the Kronecker tensor. It is convenient to divide the pressure tensor into the sensible pressure p and the trace-free part (stress tensor) $\pi_{ij} = p_{\langle ij \rangle}$, i.e. $p_{ij} = p\delta_{ij} + \pi_{ij}$. Thermodynamic temperature, sensible energy and thermal speed are defined as $T = mp/k\rho$, $e_s = 3kT/2m$ and $\theta = \sqrt{kT/m}$, where k is the Boltzmann constant and m the molecular mass. The production terms are defined as moments of the Boltzmann collision operator and there exist analytical expressions (see Truesdell & Muncaster 1980; Struchtrup 2005). Therefore, the second- and third-order production terms which correspond to the stress tensor π_{ij} and heat flux q_i rate of changes, are defined as

$$P_{ij} = \int_{\mathbb{R}^3} v'_{\langle i} v'_{j \rangle} S^{Boltz} \, \mathrm{d}V \tag{2.5}$$

and

$$P_i = \frac{1}{2} \int_{\mathbb{R}^3} v_i' v_j' v_j' S^{Boltz} \, \mathrm{d}\mathbf{V}, \tag{2.6}$$

respectively, and assuming Maxwellian molecules they become

$$P_{ij} = -\frac{p}{\mu} \pi_{ij} \tag{2.7}$$

and

$$P_i = -\frac{2}{3} \frac{p}{\mu} q_i, \tag{2.8}$$

whereas μ is the macroscopic dynamic viscosity coefficient. Here, we should clarify that the viscosity can be derived from the Boltzmann equation, but in the present FP model we regard it as a given parameter. For homogeneous moment relaxation, one obtains

$$\frac{\partial \pi_{ij}}{\partial t} = -\frac{p}{\mu} \pi_{ij} \tag{2.9}$$

and

$$\frac{\partial q_i}{\partial t} = -\frac{2}{3} \frac{p}{\mu} q_i, \tag{2.10}$$

and hence the ratio between the relaxation rates of stress and heat flux becomes $Pr = 2/3$, which is the Prandtl number. Following the same procedure for the S^{FP} operator, one obtains

$$P_{ij} = -\int_{\mathbb{R}^3} (A_i v_j' + A_j v_i' + D\delta_{ij}) \mathscr{F} \, \mathrm{d}\mathbf{V} \tag{2.11}$$

and

$$P_i = -\int_{\mathbb{R}^3} (A_i v_j' v_j' + 2A_j v_j' v_i') \mathscr{F} \, \mathrm{d}\mathbf{V} \tag{2.12}$$

with the requirement that $\int_{\mathbb{R}^3} (A_i v_j' + A_j v_i' + D\delta_{ij}) \mathscr{F} \, \mathrm{d}\mathbf{V}$ is trace-free. To further proceed, we consider $\mathbf{u}'$ as a realization from sample space $\mathbf{v}'$ and therefore $\overline{Q(\mathbf{u}')} = \int_{\mathbb{R}^3} Q(\mathbf{v}') f \, \mathrm{d}\mathbf{v}'$ which will be employed for abbreviations. As a result, the relaxation equations take the form

$$\frac{\partial \pi_{ij}}{\partial t} = -\rho \overline{A_i u_j' + A_j u_i' + D\delta_{ij}} \tag{2.13}$$

and

$$\frac{\partial q_i}{\partial t} = -\rho \overline{A_i u_j' u_j' + 2A_j u_j' u_i'} \tag{2.14}$$

and one remains with the challenge to find an appropriate formulation for the coefficients A_i and D.

2.3. *Cubic model*

For the drift coefficient, we propose a polynomial function of the fluctuating velocity, which offers enough degrees of freedom to honour consistent viscosity and Prandtl numbers. The simplest form is quadratic, but this can cause the solution to run away (see Risken 1989) and therefore the cubic model

$$A_i = \tilde{c}_{ij} v_j' + \gamma_i (v_j' v_j' - \overline{u_j' u_j'}) + \Lambda (v_i' v_k' v_k' - \overline{u_i' u_k' u_k'}) \tag{2.15}$$

is introduced here, whereas the symmetric tensor $\tilde{\boldsymbol{c}}_{ij}$, the vector $\boldsymbol{\gamma}_i$ and the scalar Λ will be determined later. By assuming $\Lambda = 0$, $\boldsymbol{\gamma}_i = 0$ and $\tilde{\boldsymbol{c}}_{ij} = -\delta_{ij}/\tau$, one obtains the simple

linear Langevin equation leading to the wrong Prandtl number $Pr = 3/2$. Therefore, here we propose a general form of these coefficients in order to fix Pr. There are two criteria that have to be studied. First, the model should recover the linear FP model in the limit of equilibrium distribution. It means the linear relaxation term has to appear in the model. Second, the stability of the equation has to be checked. The quadratic form will not be stable for any choice of macroscopic coefficients. Therefore, moving to a cubic form is necessary for stability, but not sufficient. Indeed, the coefficient Λ of the cubic term should be negative. To fulfill the mentioned criteria, we choose

$$\Lambda = -\frac{1}{\alpha \rho^3} |\det(\pi_{ij})|, \tag{2.16}$$

where $\det(\boldsymbol{\pi}_{ij})$ is the determinant of the stress tensor $\boldsymbol{\pi}_{ij}$ and $\alpha = \tau (\overline{u_i' u_i'})^4$ a scaling factor with $\tau = 2\mu/p$ the relaxation time. For the following derivations, it is helpful to decompose the linear drift term into its equilibrium and perturbation components, i.e. $\tilde{\mathbf{c}}_{ij} = -\delta_{ij}/\tau + c_{ij}$. By comparing (2.11) with (2.7) and (2.12) with (2.8), the constitutive relations

$$c_{il}\overline{u_j' u_l'} + c_{jl}\overline{u_i' u_l'} + 2\Lambda \overline{u_i' u_j' u_k' u_k'}$$
$$\boldsymbol{\gamma}_i \overline{u_l' u_l' u_j'} + \gamma_j \overline{u_l' u_l' u_i'} + D\delta_{ij} - \frac{2}{\tau}\overline{u_i' u_j'} = -\frac{p}{\mu}\overline{u_i' u_j'} + \frac{2e_s p}{3\mu}\delta_{ij} \tag{2.17}$$

and

$$\left.\begin{array}{l} 2c_{jl}\overline{u_l' u_i' u_j'} + c_{il}\overline{u_l' u_j' u_j'} \\[4pt] +2\gamma_j\overline{\left(u_l' u_l' - \overline{u_l' u_l'}\right) u_i' u_j'} \\[4pt] +\boldsymbol{\gamma}_i\overline{\left(u_l' u_l' - \overline{u_l' u_l'}\right) u_j' u_j'} \\[4pt] +2\Lambda\overline{\left(u_l' u_j' u_j' - \overline{u_l' u_j' u_j'}\right) u_l' u_i'} \\[4pt] +\Lambda\overline{\left(u_i' u_j' u_j' - \overline{u_i' u_j' u_j'}\right) u_l' u_l'} \\[4pt] -\dfrac{3}{\tau}\overline{u_i' u_j' u_j'} = -\dfrac{Pr\,p}{\mu}\overline{u_i' u_j' u_j'}. \end{array}\right\} \tag{2.18}$$

for the molecular stresses and the heat fluxes are obtained. Note that $Pr = 2/3$ for monatomic gas. In order to close the system of equations, a diffusion has to be chosen. In order to recover the linear model in the limit of equilibrium, we keep it like in the simple Langevin equation, i.e.

$$D = \sqrt{\frac{4e_s}{3\tau}}. \tag{2.19}$$

The final Fokker–Planck approximation of the Boltzmann equation for monatomic gas reads

$$\frac{\partial \mathcal{F}}{\partial t} + V_i \frac{\partial \mathcal{F}}{\partial x_i} + G_i \frac{\partial \mathcal{F}}{\partial V_i} + \frac{\partial \left((\tilde{\mathbf{c}}_{ij} v_j' + \boldsymbol{\gamma}_i (v_j' v_j' - \overline{u_j' u_j'}) + \Lambda(v_i' v_k' v_k' - \overline{u_i' u_k' u_k'}))\mathcal{F} \right)}{\partial V_i}$$
$$= \frac{\partial^2}{\partial V_j \partial V_j}\left(\frac{2e_s}{3\tau}\mathcal{F}\right), \tag{2.20}$$

whereas the coefficients c_{ij} and γ_i have to be determined by solving the system consisting of the linear equations

$$c_{il}\overline{u'_j u'_l} + c_{jl}\overline{u'_i u'_l} + \gamma_i\overline{u'_l u'_l u'_j} + \gamma_j\overline{u'_l u'_l u'_i} + 2\Lambda\overline{u'_i u'_j u'_k u'_k} = 0 \qquad (2.21)$$

and

$$2\Lambda\overline{\left(u'_l u'_j u'_j - \overline{u'_l u'_j u'_j}\right) u'_l u'_i} + \Lambda\overline{\left(u'_i u'_j u'_j - \overline{u'_i u'_j u'_j}\right) u'_l u'_l}$$

$$+2c_{jl}\overline{u'_l u'_i u'_j} + c_{il}\overline{u'_l u'_j u'_j} + 2\gamma_j\overline{\left(u'_l u'_l - \overline{u'_l u'_l}\right) u'_i u'_j}$$

$$+\gamma_i\overline{\left(u'_l u'_l - \overline{u'_l u'_l}\right) u'_j u'_j} = \frac{5}{3\tau}\overline{u'_i u'_j u'_j}. \qquad (2.22)$$

It can be seen that in the equilibrium, Λ vanishes as $\pi_{ij} = 0$. Moreover, the r.h.s. of (2.21) and (2.22) become zero and thus c_{ij} and γ_i. Therefore, the presented model equation recovers the linear FP model in the limit of equilibrium.

2.4. *Langevin equation*

The high dimensionality of the FP operator makes its direct numerical solution rather difficult. Indeed, instead of the FP model, equivalent nonlinear stochastic differential equations (SDEs) of Langevin type are solved for individual particle realizations (here the particles are statistical representatives of gas molecules). To see this connection, let us consider an ensemble of such particles whose states $(X(t), M(t))$ evolve according to

$$\frac{\mathrm{d}M_i}{\mathrm{d}t} = -\frac{1}{\tau}M'_i + c_{ij}M'_j + \gamma_i(M'_j M'_j - \overline{M'_j M'_j})$$

$$+ \Lambda(M'_i M'_k M'_k - \overline{M'_i M'_k M'_k}) + D\frac{\mathrm{d}W_i}{\mathrm{d}t} + G_i \quad (2.23)$$

and

$$\frac{\mathrm{d}X_i}{\mathrm{d}t} = M_i, \qquad (2.24)$$

where the fluctuating part of the molecular velocity is $M' = M - U$. Note that $W(t)$ with $\mathrm{d}W = W(t+\mathrm{d}t) - W(t)$ is a Wiener process, which is a rapidly changing random force with variance $\overline{\mathrm{d}W_i\,\mathrm{d}W_j} \equiv \delta_{ij}\,\mathrm{d}t$ and zero mean value $\overline{\mathrm{d}W_i} \equiv 0$. In the limit of infinitely many particle paths $\{X^\alpha, M^\alpha\}_{\alpha\in\mathbb{N}}$ (here α is the particle index) simulated according to (2.23) and (2.24), the distribution of molecular velocities M^α at a given location x and time t becomes consistent with the solution $\mathscr{F}(V, x, t)$ of the Fokker–Planck (2.21). It further leads to evaluating various velocity moments based on the ensemble of simulated particles, i.e. $\overline{Q(M)} = \int_{\mathbb{R}^3} Q(V) f\,\mathrm{d}V$, where $f(V; x, t) = \mathscr{F}(V, x, t)/\rho$. At this point, the integrity of the model clearly reveals that it provides enough freedom to control the relevant moments and it will be shown next that it allows for very efficient Monte Carlo simulations.

3. Solution algorithm

Here, an algorithm to simulate the particle evolutions according to the stochastic differential equations (2.23) and (2.24) with the constitutive relations (2.21) and (2.22) is presented. Following the line of arguments by Jenny *et al.* (2010), a method with the following properties will be devised.

(i) Without external force, mean velocity and energy are conserved.

(ii) All first and second conditional moments of velocity and position are reproduced.

(iii) The exact velocity auto-correlation coefficient is recovered.

To cope with the mentioned criteria, a very accurate numerical scheme is proposed in the following subsection.

3.1. *Numerical scheme*

Since (2.23) and (2.24) form a nonlinear stochastic system, we cannot seek for an analytical solution like for the linear Langevin model discussed by Jenny *et al.* (2010). However, in the following, we present a novel numerical scheme, which will minimize the numerical errors of the whole algorithm. Since the operator is Galilean-invariant, the mean velocity will be preserved and main attention will be given to energy conservation. At first, we focus on the velocity equation (2.23) and then the evolution of the position (2.24) will be treated separately. For simplicity, but without loss of generality, let us assume that there exists no external force, i.e. $G_i = 0$. The strategy is to split the nonlinear equation (2.23) into a simple linear Langevin part L and a nonlinear remainder N as

$$\frac{\mathrm{d}M_i}{\mathrm{d}t} = \overbrace{-\frac{1}{\tau}M_i' + D\frac{\mathrm{d}W_i}{\mathrm{d}t}}^{L_i} + \overbrace{c_{ij}M_j' + \gamma_i\left(M_j'M_j' - \overline{M_j'M_j'}\right) + \Lambda\left(M_i'M_k'M_k' - \overline{M_i'M_k'M_k'}\right)}^{\frac{1}{\tau}N_i}.$$
(3.1)

First, we consider the linear part, i.e. $\mathrm{d}M_i/\mathrm{d}t = L_i$. It has a closed solution based on Itō's calculus, which is consistent with the exact evolution of moments as shown in various reference works on stochastic processes (see Chandrasekhar 1943; Gardiner 1985). Considering that the time steps n and $n+1$ correspond to the times t and $t + \Delta t$, respectively, the proposed scheme for the velocity of a representative particle is

$$M_i^{n+1} = M_i^n + M_i'^n(\mathrm{e}^{-\Delta t/\tau} - 1) + \sqrt{A}\xi_i,$$
(3.2)

where $A = 2e_s(1 - \mathrm{e}^{-2\Delta t/\tau})/3$ arises from the analytical solution of $\mathrm{d}M_i/\mathrm{d}t = L_i$. The independent Gaussian random term is denoted by ξ_i with Normal distribution, zero mean and a variance of $\overline{\xi_i^2} = 1$. For the nonlinear part, we adopt the first-order forward Euler time integration scheme. Therefore, the full equation is integrated as

$$M_i^{n+1} = M_i^n + M_i'^n(\mathrm{e}^{-\Delta t/\tau} - 1) + \sqrt{\tilde{A}}\xi_i + \frac{\Delta t}{\tau}N_i^n.$$
(3.3)

Now, we have to find a new diffusion coefficient $\tilde{A}$ in order to conserve energy. This is a crucial step; otherwise, we would need to drastically restrict the time-step size. The operator $\langle .|. \rangle$ is introduced for conditional expectation. We have to evaluate the conditional variance

$$\langle M_i^{n+1}M_i^{n+1}|\boldsymbol{M}^n\rangle = \overline{M_i^n M_i^n} + 2\overline{M_i'^n M_i'^n}(\mathrm{e}^{-\Delta t/\tau} - 1)$$
$$+ \overline{M_i'^n M_i'^n}(\mathrm{e}^{-\Delta t/\tau} - 1)^2 + 3\tilde{A} + \left(\frac{\Delta t}{\tau}\right)^2 \overline{N_i^n N_i^n}, \quad (3.4)$$

where we have already used the fact that $\overline{M_i'N_i}$ and $\overline{M_iN_i}$ vanish. First, note that $\overline{M_iN_i} = \overline{M_i'N_i}$, since $\overline{N_i} = 0$, and consider the related second-order constitutive equation, i.e.

$$c_{il}\overline{M_j'M_l'} + c_{jl}\overline{M_i'M_l'} + \gamma_i\overline{M_l'M_l'M_j'} + \gamma_j\overline{M_l'M_l'M_i'} + 2\Lambda\overline{M_i'M_j'M_k'M_k'} = 0.$$
(3.5)

1. Particles evolve according to (3.7) and (3.8) for half a time step.
2. Boundary conditions are employed.
3. Required statistical moments are evaluated from the particles at each grid point.
4. Statistical moments are extrapolated to the particles.
5. System (B 1) of constitutive equations is solved for each grid point.
6. Constitutive coefficients are interpolated to the particles.
7. Particles evolve a full time step.
8. Repeat steps (2)–(6).
9. Go back to (1) and continue with the next time step.

TABLE 1. Computational algorithm.

By setting $i = j$, the left-hand side (l.h.s.) becomes $\overline{M'_i N_i}$ and therefore has to vanish. Going back to (3.4), we choose $\tilde{A}$ as

$$\tilde{A} = A - \left(\frac{\Delta t}{\tau}\right)^2 \frac{\overline{N_i^n N_i^n}}{3} \tag{3.6}$$

and it can be shown that this modification conserves energy. Note that $\tilde{A}$ always has to remain positive, which limits the time-step size, but in practical problems with $\Delta t \lesssim 4\tau$, the diffusion coefficient $\tilde{A}$ stays positive. The position evolution according to (2.24) should be consistent with the evolution of the joint expectations $\overline{X_i M_j}$ and $\overline{X_i X_j}$. In Appendix A, we derive an exact scheme for the position based on the velocity evolution. Here, we just present the final result, i.e.

$$M_i^{n+1} = M_i^n + M_i''^n(\mathrm{e}^{-\Delta t/\tau} - 1) + \sqrt{\tilde{A} - \frac{C^2}{B}} \xi_{i,u} + \sqrt{\frac{C^2}{B}} \xi_{i,X} + \frac{\Delta t}{\tau} N_i^n + G_i^n \Delta t \tag{3.7}$$

and

$$X_i^{n+1} = X_i^n + M_i''^n \tau(1 - \mathrm{e}^{-\Delta t/\tau}) + \sqrt{B} \xi_{i,X} + U_i \Delta t + \frac{\Delta t^2}{2\tau} N_i^n + G_i^n \Delta t^2/2 \tag{3.8}$$

with the coefficients

$$\tilde{A} = \frac{2e_s}{3}(1 - \mathrm{e}^{-2\Delta t/\tau}) - \left(\frac{\Delta t}{\tau}\right)^2 \frac{\overline{N_i^n N_i^n}}{3}, \tag{3.9}$$

$$B = \left(\frac{2e_s \tau^2}{3} + \frac{\tau^2 \overline{N_i^n N_i^n} \left(\frac{\Delta t}{\tau}\right)^2}{3(\mathrm{e}^{-2\Delta t/\tau} - 1)}\right)\left(\frac{2\Delta t}{\tau} - (1 - \mathrm{e}^{-\Delta t/\tau})(3 - \mathrm{e}^{-\Delta t/\tau})\right), \tag{3.10}$$

and

$$C = \left(\frac{2e_s \tau}{3} + \frac{\tau \overline{N_i^n N_i^n} \left(\frac{\Delta t}{\tau}\right)^2}{3(\mathrm{e}^{-2\Delta t/\tau} - 1)}\right)(1 - \mathrm{e}^{-\Delta t/\tau})^2. \tag{3.11}$$

For each computational grid, the coefficients c_{ij} and γ_i are evaluated from system of (2.21) and (2.22). The components of the system are presented in Appendix B.

Each time step of the numerical algorithm is summarized in table 1. For accurate unsteady results, iterations within each time step may be required.

3.2. *Boundary conditions*

The boundary conditions are treated in the same way as discussed by Jenny *et al.* (2010). Here, only the wall boundary condition treatment is discussed briefly as follows.

(*a*) Time and position where a particle hit the boundary is determined.
(*b*) The particle is positioned at that intersection point.
(*c*) The remaining time is calculated.
(*d*) Statistical moments are interpolated to the particle position.
(*e*) The particle velocity is determined from the proper PDF.
(*f*) The particle evolves for the remaining time.

In the trivial case of specular reflection, no statistical modelling for the wall treatment is required. The velocity component normal to the wall is simply reversed and the tangential ones remains unaffected. Isothermal wall modelling is more challenging. While the tangential components are sampled from local Maxwellian distributions with zero mean and variance $\theta_w^2 = kT_w/m$ (T_w is the wall temperature and θ_w the thermal velocity), the wall-normal velocity M_n shall be sampled from a distribution corresponding to the inward flux of a Maxwellian distribution (Jenny *et al.* 2010), i.e.

$$f(v) = \frac{H(v)v}{C} e^{-v^2/(2\theta_w^2)}, \tag{3.12}$$

with $H(.)$ as the Heaviside function and $1/C$ being the normalization factor. Note that f is defined over the sample space v which has a direction towards the computational domain. In order to generate a particle velocity from (3.12), we consider the inverse of the cumulative distribution function $F(v) = \int_{-\infty}^{v} f(m)\mathrm{d}m$, i.e.

$$F(v) = e^{-v^2/(2\theta_w^2)}. \tag{3.13}$$

Further, we may generate a random fraction R_f (uniformly distributed random number between 0 and 1) and set it equal to $F(v)$. Consequently, the desired wall-normal component of the particle velocity can be sampled as $M_n = \pm \theta_w \sqrt{-2\ln(R_f)}$ which depending on the inward direction, $+$ or $-$ is chosen. The same procedure is employed in DSMC for initializing the particle velocity after hitting the isothermal wall (Bird 1994). The difference is indeed in the subsequent evolution of the particle for the remaining time where in DSMC it continues along a straight line but for FP it otherwise follows (3.7) and (3.8). After enforcing the boundary conditions, there is a possibility that the particle again hits the wall and in that case the algorithm has to be repeated. Note that using the diffuse wall boundary condition, proposed by Maxwell, may lead to certain limitations (see e.g. Sharipov 2002); however, for the current study this model was employed.

3.3. *Statistical moments*

The estimation of statistical moments plays a significant role in terms of computational efficiency. For statistically stationary problems, a relatively cheap and efficient algorithm was proposed by Jenny *et al.* (2001), which is based on a time-weighted averaging method. Suppose that $\tilde{\beta}$ is a quantity representing the estimation of a statistical moment like $u_{i_1,i_2,\dots,i_n}^{(p)}$ which is an ensemble average of the particle velocity product $M_{i_1,i_2,\dots,i_n}^{(p)} = |\boldsymbol{M}'|^p M_{i_1}' M_{i_1}' \dots M_{i_n}'$. To better understand, we consider $\mathscr{W}(\boldsymbol{x}^l, t)$ as an estimation of the number of particles at position $\boldsymbol{x}^l$ in the computational cell $l \in \{1, \dots, N_n\}$ and time t. Therefore, the updated estimation of that for time step $J + 1$ using the positions $\boldsymbol{X}^j$, $j \in \{1, \dots, N_p\}$ of all the particles

will be

$$\mathscr{W}^{J+1}(\boldsymbol{x}^l, t) = \mu \mathscr{W}^J(\boldsymbol{x}^l, t) + (1 - \mu) \sum_{j=1}^{N_p} \{g^l(\boldsymbol{X}^j(t))\}, \tag{3.14}$$

where $\mu = 1 - 1/n_a$ is the weight factor and n_a characterizes the number of steps over which it is averaged. The kernel $g^l(\boldsymbol{x})$ was introduced with the constraint

$$\sum_{l=1}^{N_n} g^l(\boldsymbol{x}) \equiv 1 \qquad \forall \boldsymbol{x} \in \Omega \tag{3.15}$$

for interpolation. The same procedure can be adopted to update the weighted ensemble averages $\mathscr{S}(\boldsymbol{x}^l, t)$, i.e.

$$\mathscr{S}^{J+1}(\boldsymbol{x}^l, t) = \mu \mathscr{S}^J(\boldsymbol{x}^l, t) + (1 - \mu) \sum_{j=1}^{N_p} \{g^l(\boldsymbol{X}^j(t))(M^{(p)}_{i_1, i_2, \ldots, i_n})^j\}. \tag{3.16}$$

Finally, the updated velocity moment will be obtained as

$$\tilde{\beta}^{J+1} = \frac{\mathscr{S}^{J+1}}{\mathscr{W}^{J+1}}. \tag{3.17}$$

For unsteady problems, the above-mentioned method should not be used. There, the only way towards reducing statistical and bias errors is to increase the number of particles.

3.4. *Numerical validation*

We now compare the accuracy of the proposed scheme with a conventional finite-difference (FD) method. Using simple FD gives rise to the discretization

$$M_i^{n+1} - M_i^n = \left(\left(-\frac{M''^n_i}{\tau^n} + c_{ij}^n M''^n_j + \gamma_i^n (M''^n_j M''^n_j - 2e_s{}^n)\right.\right.$$
$$\left.\left. + \Lambda^n (M''^n_j M''^n_l M''^n_l - \overline{M''^n_j M''^n_l M''^n_l})\right) \Delta t + \sqrt{\frac{4e_s{}^n}{3\tau^n}} \Delta t \xi_i\right) \left(1 - \frac{\Delta t}{2\tau^n}\right) \tag{3.18}$$

and

$$X_i^{n+1} - X_i^n = \frac{\Delta t}{2}(M_i^{n+1} + M_i^n) \tag{3.19}$$

of the nonlinear equations (3.7) and (3.8). Relaxation of a gas in non-equilibrium is considered. The initial velocity PDF is described by the superposition of three Gaussian PDFs, i.e.

$$f(\boldsymbol{V}) = \frac{1}{3\pi^{1.5}}(e^{-(\boldsymbol{V}-\boldsymbol{p}_1).(\boldsymbol{V}-\boldsymbol{p}_1)} + e^{-(\boldsymbol{V}-\boldsymbol{p}_2).(\boldsymbol{V}-\boldsymbol{p}_2)} + e^{-(\boldsymbol{V}-\boldsymbol{p}_3).(\boldsymbol{V}-\boldsymbol{p}_3)}). \tag{3.20}$$

The local mean values of the three modes are denoted by the vectors $\boldsymbol{p}_k$ ($k \in \{1, 2, 3\}$), which are chosen such that the mean velocity is zero; we chose $\boldsymbol{p}_1 = (5\sqrt{3}, -5, 0) \, \mathrm{m\,s^{-1}}$, $\boldsymbol{p}_2 = (-5\sqrt{3}, -5, 0) \, \mathrm{m\,s^{-1}}$ and $\boldsymbol{p}_3 = (0, 10, 0) \, \mathrm{m\,s^{-1}}$. Further, we assume homogeneity without external forces, i.e. $G_i = 0$ and consequently e_s and τ have to remain constant. To evaluate that the proposed method preserves energy, we calculate e_s from the particle ensemble after every time step. To keep the statistical errors small, we employ $N_p = 10^5$ particles. Different time-step sizes $\Delta t \in \{\tau/16, \tau/4, 2\tau, 4\tau\}$ for the proposed scheme and $\Delta t \in \{\tau/16, \tau/4, \tau\}$ for the FD integration were employed to ensure that
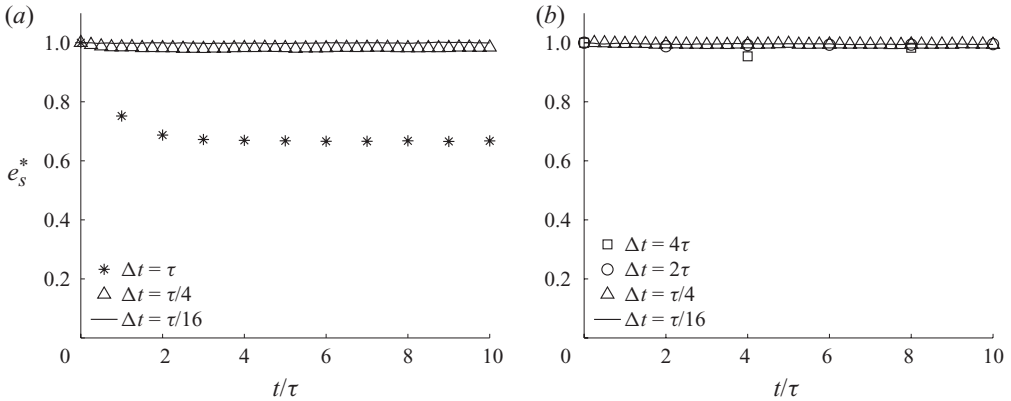
FIGURE 1. $e_s^* = e_s/\theta^2$ for $t/\tau \in [0, 10]$ with the common scheme (*a*) and with the new scheme (*b*). For both schemes, different time steps are employed, i.e. $\Delta t/\tau \in \{\frac{1}{16}, \frac{1}{4}, 1\}$ for the common scheme and $\Delta t/\tau \in \{\frac{1}{16}, \frac{1}{4}, 2, 4\}$ for the new scheme.
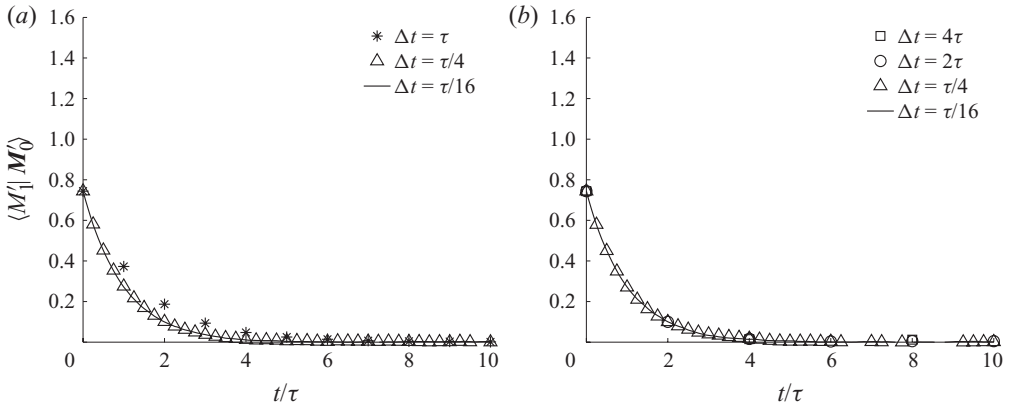

FIGURE 2. $\langle M_1' | M_0' \rangle$ for $t/\tau \in [0, 10]$ with the common scheme (left) and with the new scheme (right). For both schemes different time steps are employed, i.e. $\frac{\Delta t}{\tau} \in \{\frac{1}{16}, \frac{1}{4}, 1\}$ for the common scheme and $\frac{\Delta t}{\tau} \in \{\frac{1}{16}, \frac{1}{4}, 2, 4\}$ for the new scheme.

the proposed scheme gives more accurate results for even larger time-step sizes. The superiority of the new scheme is clearly demonstrated in figures 1(*a*) and 1(*b*). The FD method suffers from numerical dissipation (figure 1*a*), while the new method (figure 1*b*) conserves energy independent of the time-step size. Note that normalizations are adopted based on thermal speed θ as a reference velocity and τ as a reference time scale. Conditional expectations are examined for particles with initial velocity $M_0' = (\theta, 0, 0)$, whereas the macroscopic coefficients are assumed to remain constant during the simulation time. The results computed with the new scheme are shown in figures 2(*b*), 3(*b*), 4(*b*), 5(*b*) and 6(*b*), and those computed with the conventional FD method are depicted in the figures 2(*a*), 3(*a*), 4(*a*), 5(*a*) and 6(*a*). Comparisons reveal that new scheme is much more accurate and consistent than FD integration.

4. Results and discussions

In this section, for verification, the presented collision model is compared with DSMC for different force-driven micro-channel flows with isothermal walls. The
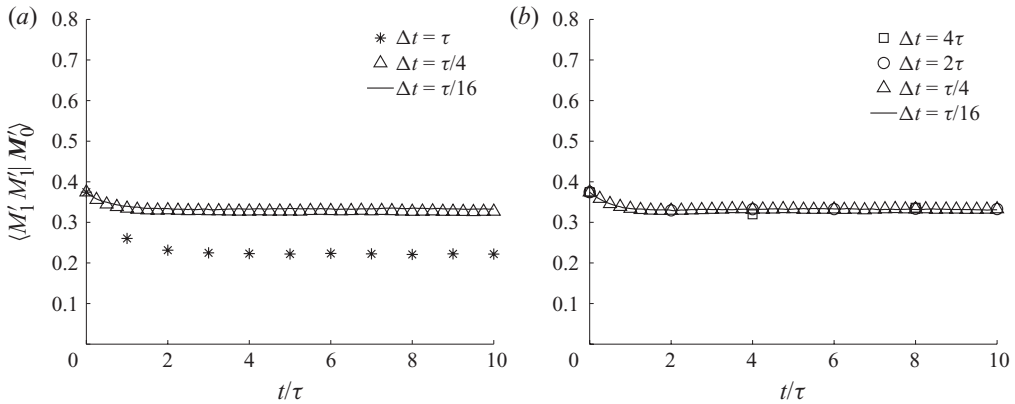
FIGURE 3. $\langle M_1 M_1 | M'_0 \rangle$ for $t/\tau \in [0, 10]$ with the common scheme (a) and with the new scheme (b). For both schemes, different time steps are employed, i.e. $\Delta t/\tau \in \{\frac{1}{16}, \frac{1}{4}, 1\}$ for the common scheme and $\Delta t/\tau \in \{\frac{1}{16}, \frac{1}{4}, 2, 4\}$ for the new scheme.
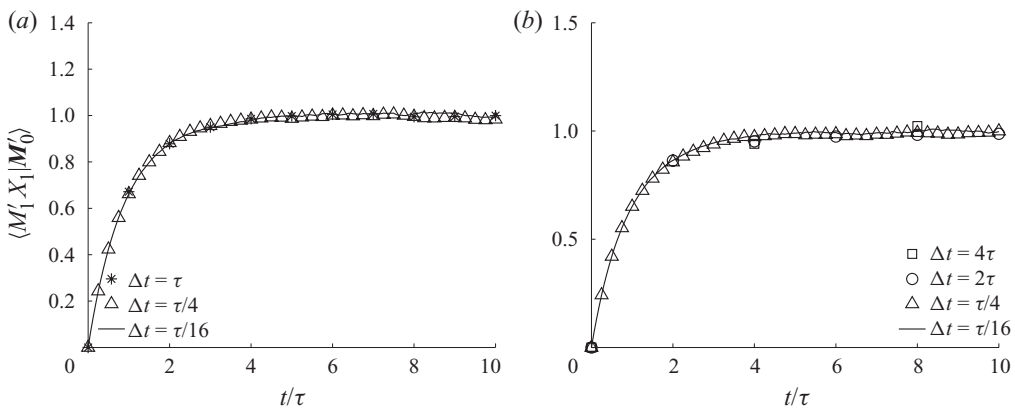

FIGURE 4. $\langle M'_1 X_1 | M'_0 \rangle$ for $t/\tau \in [0, 10]$ with the common scheme (a) and with the new scheme (b). For both schemes, different time steps are employed, i.e. $\Delta t/\tau \in \{\frac{1}{16}, \frac{1}{4}, 1\}$ for the common scheme and $\Delta t/\tau \in \{\frac{1}{16}, \frac{1}{4}, 2, 4\}$ for the new scheme.

DSMC results are based on the algorithm described by Bird (see Bird 1994) and implemented for Maxwellian molecules. The DSMC code has been developed by the authors for one-dimensional flow geometries and relevant validations have been performed. First, the effect of Maxwell (Ma) and Knudsen (Kn) numbers on the PDF shape evolution was studied. Therefore, the corresponding joint PDFs at the left channel wall were used as initial conditions for homogeneous simulations. Second, the mass flow rate as a function of Kn was investigated and the classical Knudsen paradox could be accurately reproduced up to very large Knudsen numbers. Finally, to investigate heat transport phenomena, the same micro-channel configuration with different wall temperatures on both sides was considered. It could be demonstrated that the correct heat flux and temperature distributions can be predicted for very large Knudsen numbers.
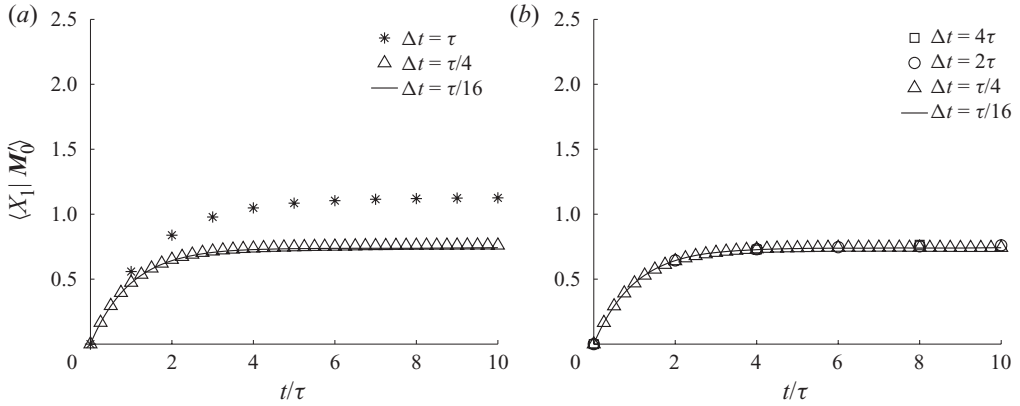
FIGURE 5. $\langle X_1 | M_0' \rangle$ for $t/\tau \in [0, 10]$ with the common scheme (a) and with the new scheme (b). For both schemes, different time steps are employed, i.e. $\Delta t/\tau \in \{\frac{1}{16}, \frac{1}{4}, 1\}$ for the common scheme and $\Delta t/\tau \in \{\frac{1}{16}, \frac{1}{4}, 2, 4\}$ for the new scheme.
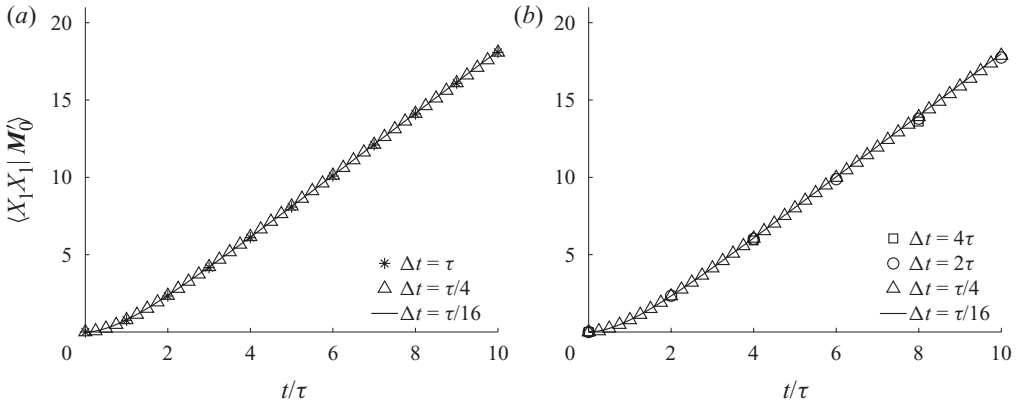

FIGURE 6. $\langle X_1 X_1 | M_0' \rangle$ for $t/\tau \in [0, 10]$ with the common scheme (a) and with the new scheme (b). For both schemes, different time steps are employed, i.e. $\Delta t/\tau \in \{\frac{1}{16}, \frac{1}{4}, 1\}$ for the common scheme and $\Delta t/\tau \in \{\frac{1}{16}, \frac{1}{4}, 2, 4\}$ for the new scheme.

4.1. *Description of test cases*

The micro-channel test case is set up as described by Jenny *et al.* (see Jenny *et al.* 2010). Vertical flow (in x_2-direction) driven by the external force $\boldsymbol{G} = (0, G, 0)^{\mathrm{T}}$ between two parallel walls is considered. Consequently, velocity and temperature gradients in the cross-stream direction (x_1-direction) are expected. Argon as monatomic gas with a molecular weight of $m = 66.3 \times 10^{-27}$ kg was chosen and standard temperature and pressure were set at $T_0 = 273$ K and $p_0 = 101\,325$ Pa, respectively. For the dynamic viscosity, the constitutive relation $\mu = 2.117 \times 10^{-5} (T/T_0)^{0.81}$ was employed and the mean free path length is defined as $\lambda = \mu \sqrt{\theta}/p$. Based on the definition of λ, the distance L between the two parallel walls can be calculated for any given Knudsen number. Note that, for convenience, the normalized force $\hat{G} = GL/\theta_w$ will be considered, whereas $\theta_w = \sqrt{kT_w/m}$ is the thermal speed based on the wall temperature T_w. In all test cases, isothermal wall-boundary conditions were applied. While for the first series of test cases, the left and right wall temperatures T_L and T_R, respectively, are both equal to 273 K, i.e. $T_L = 2T_R = 273$ K in the last test case. Since infinitely
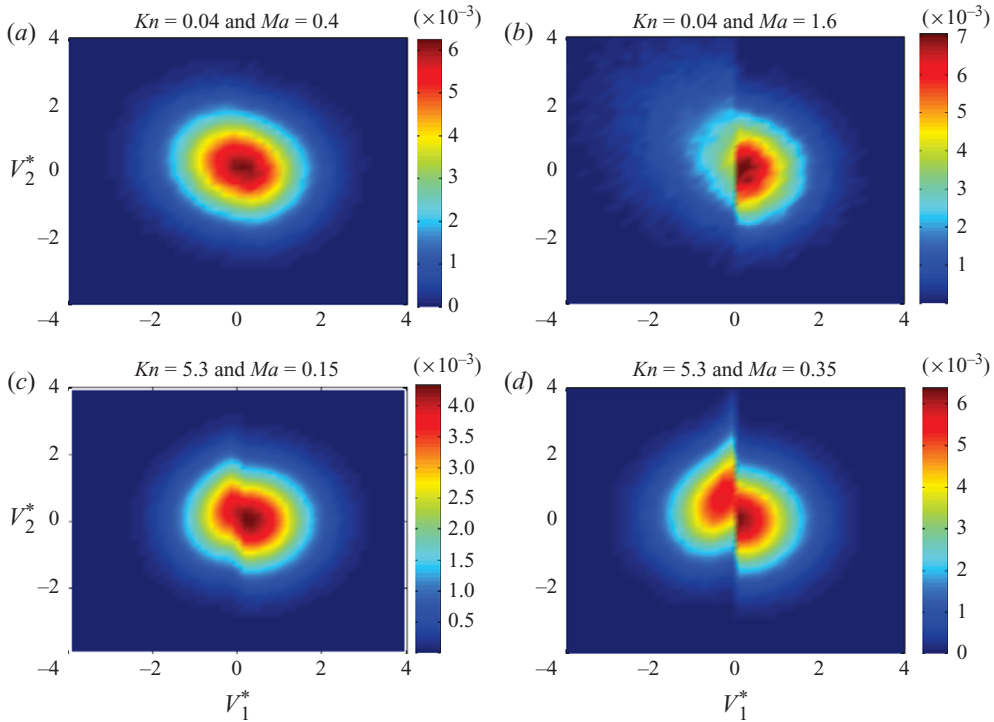
FIGURE 7. Depicted are the normalized (red: maximum value; blue: zero) velocity PDF contours near the wall for different Kn and $\hat{G}$. (a): {$Kn = 0.04$, $\hat{G} = 0.235$ & $Ma = 0.4$}; (b): {$Kn = 0.04$, $\hat{G} = 2$ & $Ma = 1.6$}; (c): {$Kn = 5.3$, $\hat{G} = 0.1$ & $Ma = 0.15$}; (d): {$Kn = 5.3$, $\hat{G} = 0.235$ & $Ma = 0.35$}.

long channels are considered, periodic boundary conditions were applied at in- and outflow of the computational domain, which is discretized into 32 equidistant grid cells, each containing on average $N_p = 50$ computational particles.

4.2. *Homogeneous relaxation*

To investigate the validity of the Fokker–Planck approximation for different Kn and Ma numbers, the relaxation of velocity PDFs in a homogeneous environment is studied. Therefore, the PDFs obtained at the left wall from micro-channel flow simulations with different Kn and Ma numbers were used as initial conditions. Note that these initial PDFs approach isotropic Maxwellian distributions, if $Ma \to 0$ and $Kn \to 0$, but deviate significantly from equilibrium for larger Ma and Kn numbers. Figure 7 shows the steady-state velocity PDF contours for $Kn = 0.04$ and $Kn = 5$ and different (maximum) Mach numbers obtained at the left micro-channel wall from DSMC. In order to control Ma, different external forces were applied, i.e. $\hat{G} = 0.235$, $\hat{G} = 2$ and $\hat{G} = 0.1$ (the maximum Mach numbers were calculated *a posteriori* from the steady-state solution). Considering the particles reflected from the wall (corresponding to the right portion of PDFs), it is shown that they all adopt a half Maxwellian distribution which is due to the isothermal boundary condition. The differences show up in the left half of the PDFs. Since larger Ma numbers lead to larger temperature jumps, an increase of the external force leads to more scattering. Note that the left portion belongs to the molecules propagating towards the wall. This
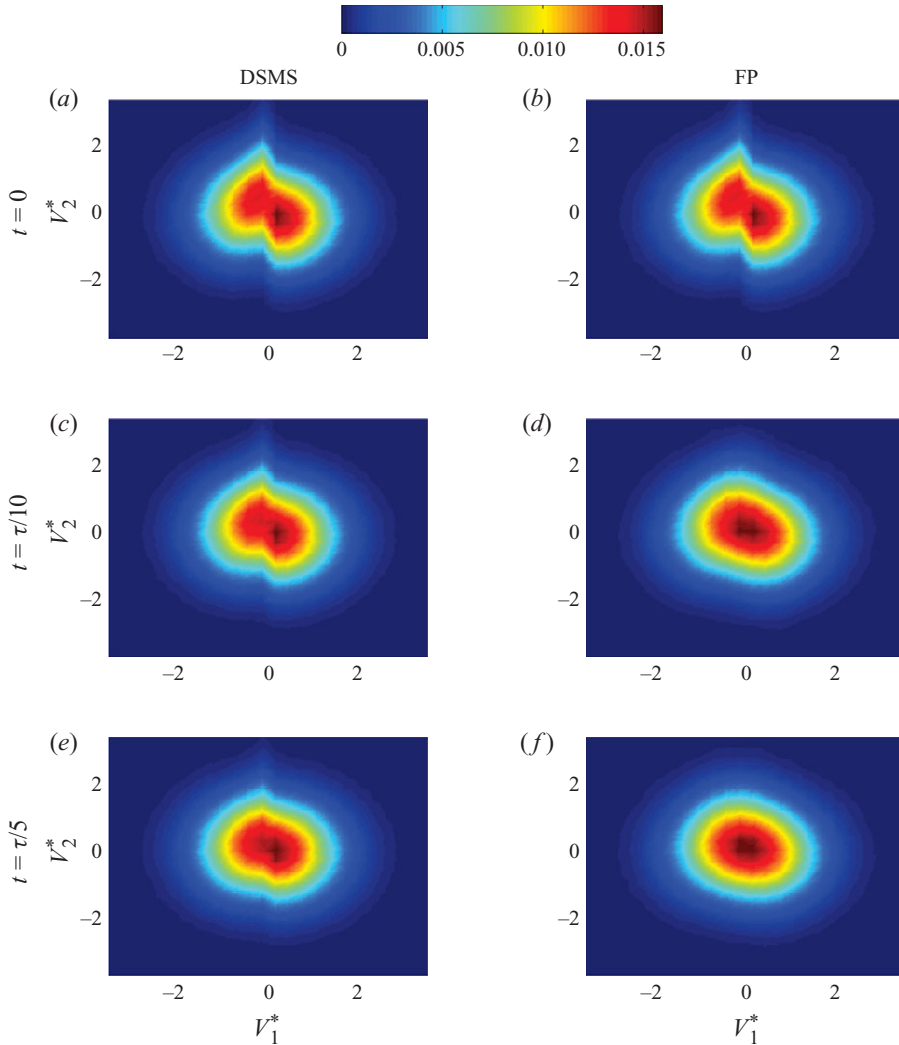
FIGURE 8. (*a–f*) Homogeneous relaxation using DSMC and FP: depicted are the normalized (red: maximum value; blue: zero) velocity PDF contours. The time interval between successive maps is $\tau/10$.

effect of Ma on the PDF shape shows that deviation from equilibrium is not only a function of Kn, but also of Ma. For example, note that only the PDF with low Kn and low Ma, i.e. that with $Ma = 0.4$ and $Kn = 0.04$ shown in figure 7, is very close to Maxwellian. On the other hand, as we increase the Knudsen number or the external force, the departure from Maxwellian velocity distribution becomes more prominent. For the cases with $\{Kn = 0.04$ and $Ma = 1.6\}$ and $\{Kn = 5.3$ and $Ma = 0.35\}$, some strong non-equilibrium features can be observed in the PDFs. Relaxations of the latter PDF with the FP model and DSMC are shown in figure 8. The discrepancy between the results is a direct consequence of the fact that jump processes are approximated by continuous drift and diffusion processes in the FP model. Note, however, that the coefficients in the FP model are constructed such that the evolution of second joint moments and heat fluxes is exact in homogeneous scenarios (like in DSMC).
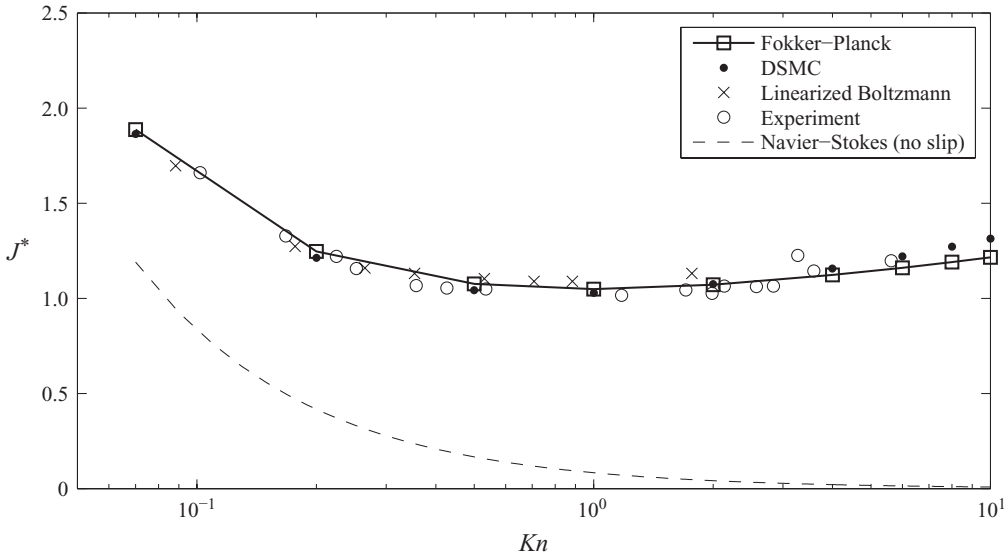
FIGURE 9. Knudsen paradox depicted are normalized mass flow rates $J^* = J/(\theta_w \hat{G} L \rho_0)$ as functions of the reference Knudsen number. The experimental data are from Dong (1956) and the linearized Boltzmann results from Ohwada *et al.* (1989).

4.3. *Poiseuille flow in slip regime*

Variation of the mass flow rate

$$J = \int_0^L \rho U_2 \, dx_1, \qquad (4.1)$$

as a function of Kn is shown in figure 9 and a very good agreement between the FP model results and the experimental data by Dong (1956) can be observed up to $Kn = 4$. It is encouraging to see that for large Knudsen numbers the FP model leads to better agreement with experiment and DSMC than linearized Boltzmann calculations from Ohwada, Sone & Aoki (1989) by using hard sphere molecules. Moreover, while Navier–Stokes with no-slip boundary conditions depicted here for general comparisons, cannot predict the flux minimum at $Kn \approx 1$, it is captured very accurately by the FP model. However, it should also be noted that Navier–Stokes equations with the proper velocity-slip boundary condition, e.g. Cercignani's second-order slip model (Cercignani 1964) provides much more accurate results in the mentioned problem (Hadjiconstantinou 2003). Detailed comparisons between DSMC and FP for the case of $Kn = 0.2$ and $Kn = 0.5$ are shown in figures 10 and 11, respectively. A very good agreement for $Kn = 0.2$ and close behaviour for $Kn = 0.5$ can be observed. For example, the FP model correctly predicts velocity slip temperature jump at the channel walls, and the local temperature minimum in the centre of the channel. The latter is a phenomenon which cannot be captured by a Navier–Stokes–Fourier system, even if the correct velocity slip and temperature jump are imposed at the wall boundaries (see Zheng, Garcia & Alder 2002; Xu 2003, 2004; Taheri, Torrilhon & Struchtrup 2009).

In order to study field quantities of flows with higher reference Knudsen numbers, in the following subsection another test case with an imposed temperature difference between left and right walls is considered.
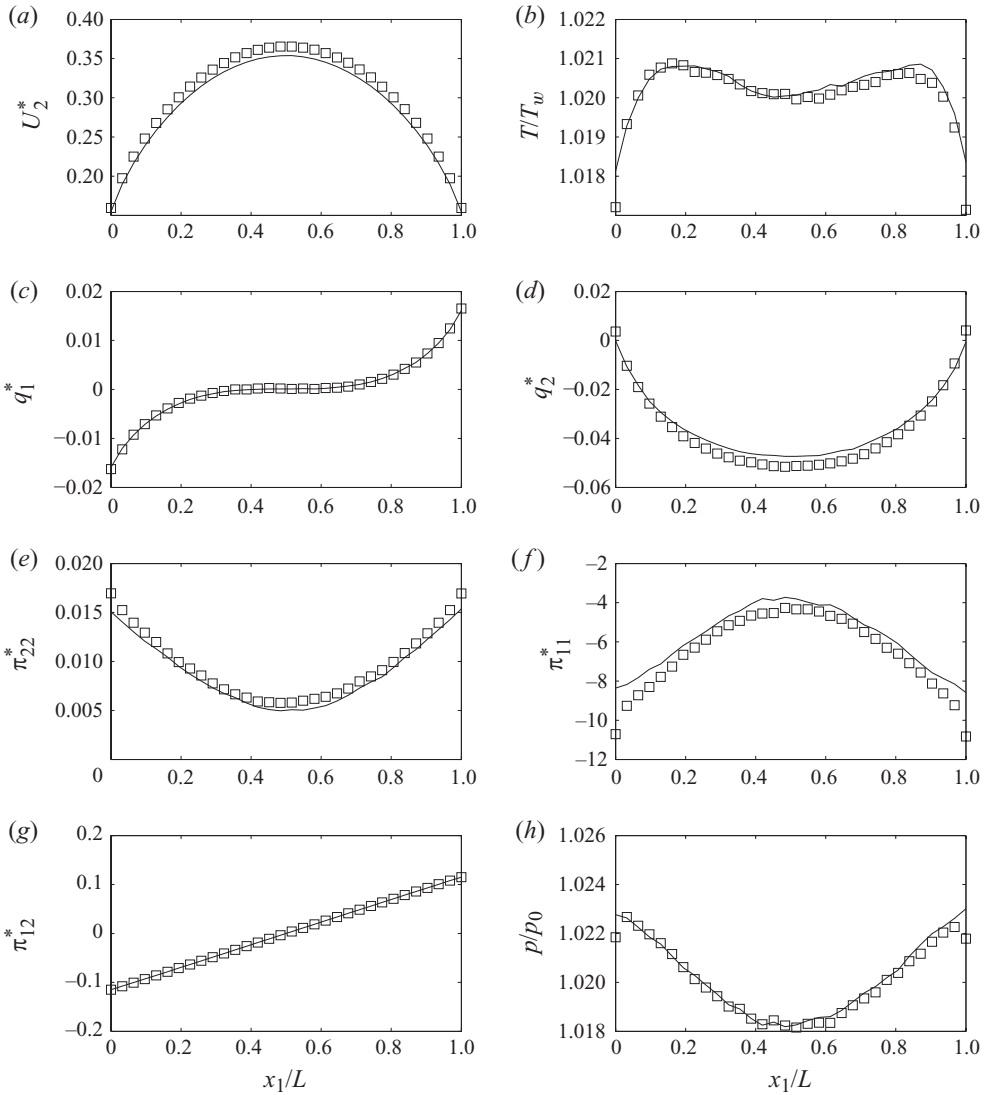
FIGURE 10. (a–h) Force-driven Poiseuille flow at $Kn = 0.2$: depicted are normalized mean velocity $U_2^* = U_2/(\theta_w \hat{G})$, normalized temperature T/T_w, normalized stress components $\pi_{ij}^* = \pi_{ij}/(\theta_w^2)$, normalized heat fluxes $q_i^* = q_i/(\theta_w^3)$ and normalized pressure p/p_0 along the cross-stream direction x_1/L. Circles indicate DSMC and solid lines FP results.

4.4. *Heat transport*

Here, the classical problem of heat transport between parallel plates is considered. The set-up is the same as in the previous test case, except that different wall temperatures are imposed, i.e. $T_L = 2T_R = T_w$ as mentioned earlier. This test case has been employed in the past for various studies with small temperature differences (see Springer 1971; Sharipov & Seleznev 1998; Torrilhon & Struchtrup 2009). As we do not make any linearizations, however, a large temperature difference is applied here. FP and DSMC solutions were calculated for $Kn = 1$ and $Kn = 2$ whereas the external force was kept small, i.e. $\hat{G} = 0.05$. Figures 12 and 13 show profiles of steady-state field quantities for $Kn = 1$ and $Kn = 2$, respectively, and comparison shows that the two methods lead to
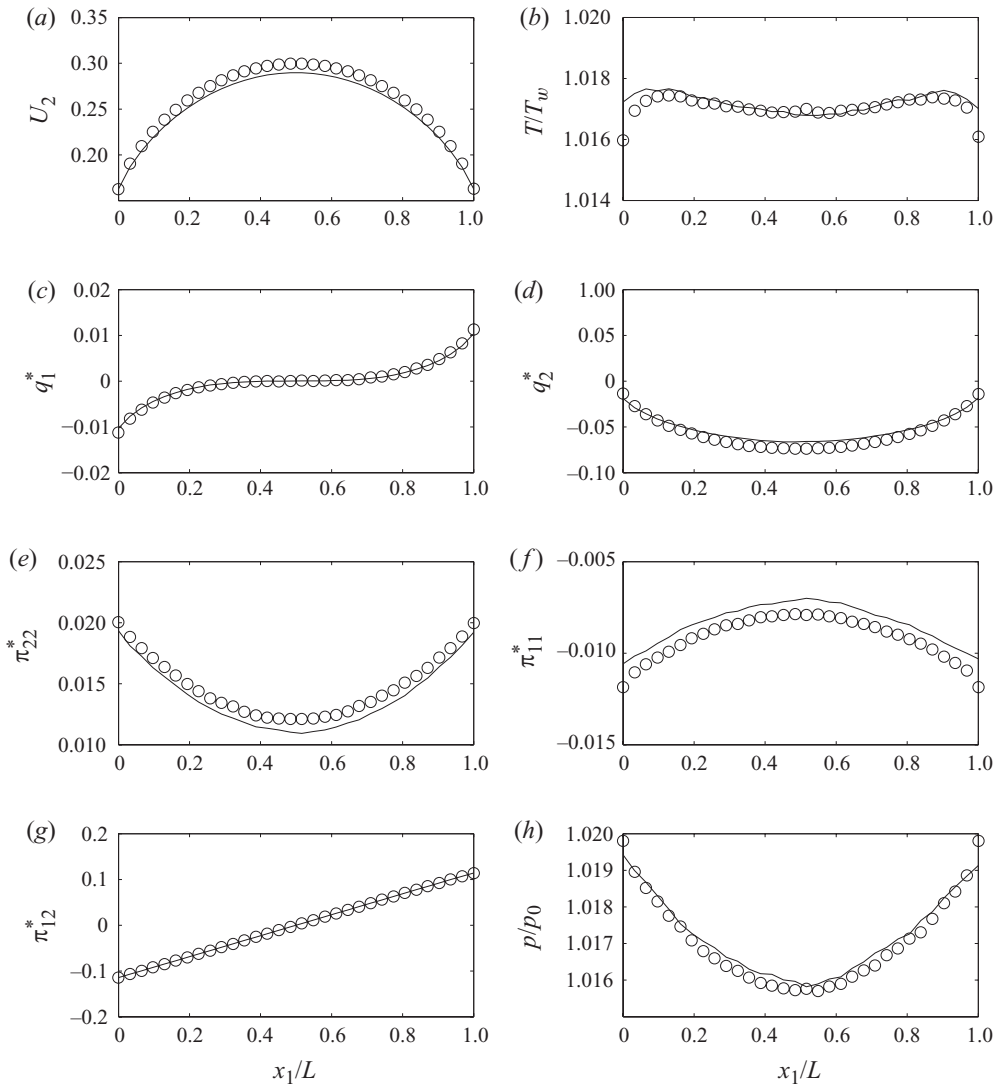
FIGURE 11. $(a–h)$ Force-driven Poiseuille flow at $Kn = 0.5$: depicted are normalized mean velocity $U_2^* = U_2/(\theta_w \hat{G})$, normalized temperature T/T_w, normalized stress components $\pi_{ij}^* = \boldsymbol{\pi}_{ij}/(\theta_w^2)$, normalized heat fluxes $q_i^* = q_i/(\theta_w^3)$ and normalized pressure p/p_0 along the cross-stream direction x_1/L. Circles indicate DSMC and solid lines FP results.

almost identical solutions. This is encouraging, especially since the Knudsen numbers are quite large here.

4.5. *Discussion of computational efficiency*

Besides comparisons between DSMC and FP regarding their accuracy, their computational costs are also of major interest. Generally, apart from the number of particles N_p, which is a key parameter, the cost of DSMC scales with the number of collisions $N_c = N_p \nu \Delta t/2$, where ν stands for collision frequency and Δt for the time-step size. The collision frequency depends on p/μ and therefore in high-density flows
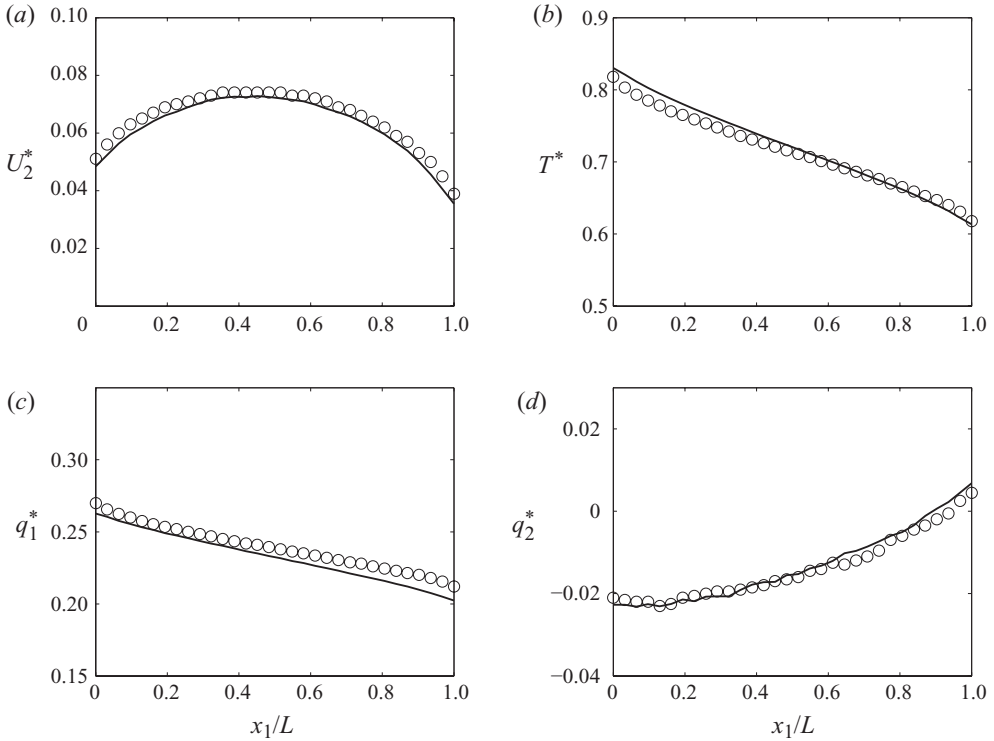
FIGURE 12. (a–d) Force-driven Poiseuille flow with $Kn = 1$ and different wall temperatures: depicted are normalized mean velocity $U_2^* = U_2/(\theta_w \hat{G})$, normalized temperature $T^* = T/T_L$ and normalized heat fluxes $q_i^* = q_i/(\theta_w^3)$ along the cross-stream direction x_1/L. Circles indicate DSMC and solid lines FP results.

usually a large number of collisions need to be considered at each time step. This leads to a very high computational cost, in particular, in the low-Knudsen-number regime.

In contrast, the cost of the FP model scales with the number of time steps and therefore, with the proposed particle time integration scheme, the efficiency of the method becomes independent of the collision frequency. As a direct consequence, for moderate Knudsen numbers, this allows for much faster simulations compared to DSMC.

To better assess the computational efficiency that would be gained by using the proposed solution algorithm, a comparison has been done on the CPU-time consuming by FP and DSMC for Poiseuille flow scenario with constant wall temperatures described in § 4.1, during one time step. It was carried out by employing the same spatial and temporal descretizations for both FP and DSMC; hence, this comparison does not embody the computational advantages of the presented method comprehensively. However, this would give a rough idea about the speed of the algorithms. The test has been performed for different number of particles, i.e. $N_p \in \{50, 100, 500, 5000, 10^4, 10^5\}$ per computational cell and different Kn, i.e. $Kn \in \{0.01, 0.05, 0.1\}$. Results shown in figure 14, reveal that the FP model admits much faster simulations which for lower Kn become more prominent, as was mentioned before.

A further advantage of the FP model is that for steady-state problems, exponentially weighted moving time averaging can be employed (as described in § 3.3) to drastically
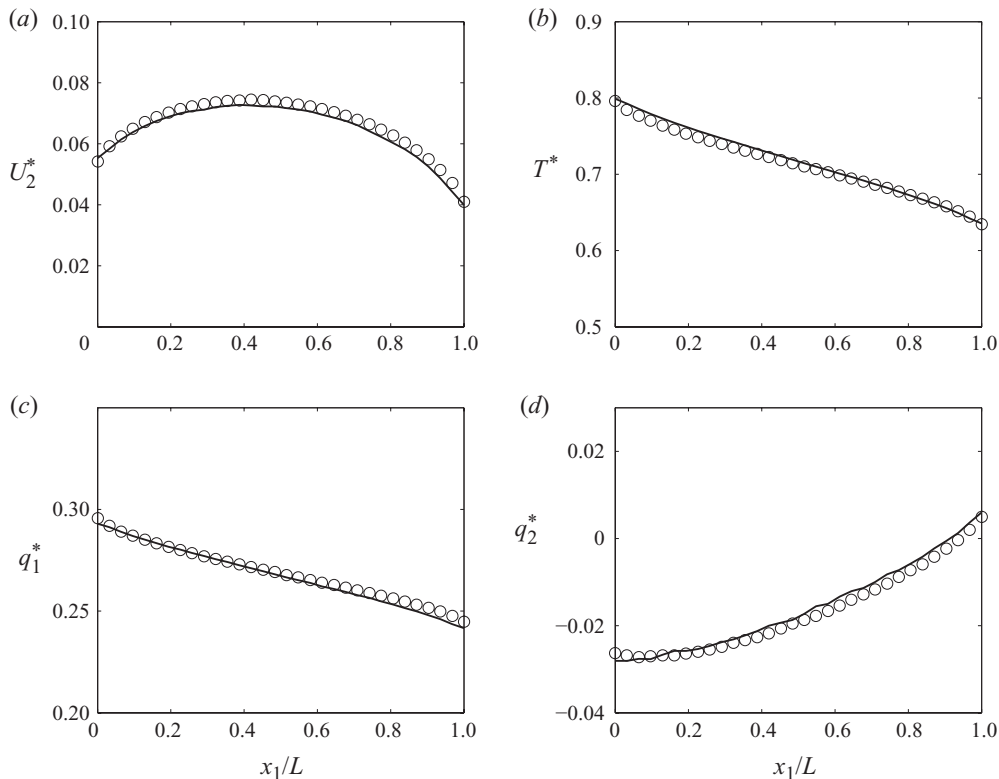
FIGURE 13. (*a–d*) Force-driven Poiseuille flow with $Kn = 2$ and different wall temperatures: depicted are normalized mean velocity $U_2^* = U_2/(\theta_w \hat{G})$, normalized temperature $T^* = T/T_L$ and normalized heat fluxes $q_i^* = q_i/(\theta_w^3)$ along the cross-stream direction x_1/L. Circles indicate DSMC and solid lines FP results.

reduce the number of computational particles while keeping statistical and bias errors constant. This leads to a tradeoff between an increased number of required time steps due to the induced time lag and computational gain per time step due to a decrease of the required particle number. In general, however, this technique proved to significantly reduce the simulation times. Note that although the exponentially weighted moving time averaging reduces the statistical error in DSMC, it cannot be employed there to control the deterministic bias error. As the FP model, in the presented algorithm, is solved by using stochastic particle methods, similar barriers like DSMC would be faced concerning unsteady flow simulations. However, it is interesting to note that as in the FP framework particles follow independent stochastic paths, therefore, in contrast to DSMC (see Dagum 1991), very efficient parallel implementations of the algorithm can be achieved.

Rarefied gas flows in higher dimensional geometries would be handled by the FP model with a relatively cheap computational cost. For example, the flow around a cylinder has been simulated by Jenny *et al.* (2010), employing linear drift coefficient, where they have shown that major flow gradients can be captured even by using very coarse spatial grids. Therefore, the algorithm would deal with complex geometries very easily which is not surprising as the governing equations here are solved through particles.
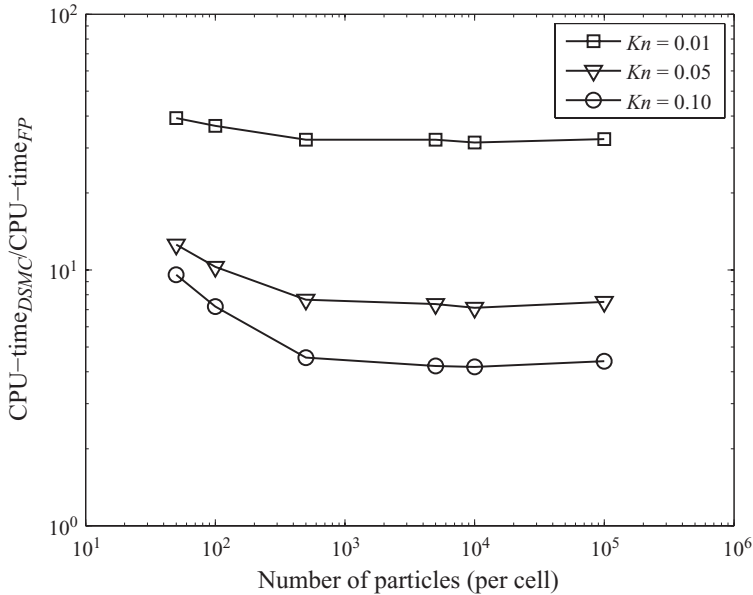
FIGURE 14. CPU-time comparison between DSMC and FP. Depicted is the ratio of the CPU-times between DSMC and FP for different $Kn \in \{0.01, 0.05, 0.1\}$ employing different particle numbers, i.e. $N_p \in \{50, 100, 500, 5000, 10^4, 10^5\}$ per computational cell. Note that an identical time-step size and grid spacing have been used for both.

5. Conclusion

In this paper, an extension of the gas-kinetics approximation presented by Jenny *et al.* (2010) is proposed, which leads to the correct Prandtl number of 2/3 for monatomic gas molecules. This was achieved by introducing a cubic drift term in the stochastic particle model. Moreover, an accurate and energy conserving solution algorithm was devised in order to allow for large time steps.

Different aspects of the presented FP model were investigated, in which force-driven Poiseuille flows were considered. From the good agreement with DSMC and experiments, at least for low Mach numbers, it can be concluded that the continuous stochastic processes for the particle velocities are suitable for simulations of rarefied gas flows from very small up to quite high Knudsen numbers.

In terms of efficiency, the FP-based solution algorithm is far superior than collision-based algorithms like DSMC, which is due to the independent particle evolutions in the FP model, smaller number of required particles and large time steps which can be employed.

Appendix A. Postition evolution

The position evolution scheme should be calculated by using time integration of the particle velocity, i.e.

$$\Delta X_i = \int_0^{\Delta t} M_i \, \mathrm{d}t. \tag{A 1}$$

For simplicity, but without loss of generality, we consider an ensemble of particles without mean velocity, i.e. $\boldsymbol{M} = \boldsymbol{M}'$. Before deriving the position evolution scheme, we need to find a modified Langevin-type equation in order to compensate the error introduced by the time integration of the nonlinear term in the velocity equation. Let us assume that we have a modified diffusion coefficient $\tilde{D} = D^2 + f$. In that case, without external force, the nonlinear Langevin equation becomes

$$\frac{\mathrm{d}M_i}{\mathrm{d}t} = -\frac{1}{\tau}M_i + \sqrt{\tilde{D}}\frac{\mathrm{d}W_i}{\mathrm{d}t} + N_i. \qquad (A\,2)$$

Assuming N_i to be independent of time, the solution of (A 2) reads (see Chandrasekhar 1943)

$$M_i^{n+1} = M_i^{\,n}\mathrm{e}^{-\Delta t/\tau} + \lim_{N\to\infty}\sum_{k=1}^{N}\xi_{k,i}\sqrt{(D^2+f)\left(\frac{\Delta t}{N}\right)}\mathrm{e}^{-k\Delta t/N\tau} + N_i\left(\frac{\Delta t}{\tau}\right). \qquad (A\,3)$$

Now, we have to calculate the evolution of the velocity variance

$$\langle M_i^{n+1}M_i^{n+1}|\boldsymbol{M}^n\rangle = 3f\int_0^{\Delta t}\mathrm{e}^{\frac{-2\Delta t}{\tau}}\,\mathrm{d}t + \frac{\overline{N_i^{\,n}N_i^{\,n}}}{\tau^2}\Delta t^2. \qquad (A\,4)$$

As there is no external force, we need to fulfill the conservation of energy, which leads to

$$f = -\frac{\overline{N_i^n N_i^n}\left(\dfrac{\Delta t}{\tau}\right)^2}{\dfrac{3\tau}{2}(\mathrm{e}^{-2\Delta t/\tau}-1)}. \qquad (A\,5)$$

Now, the modified stochastic velocity equation becomes

$$\frac{\mathrm{d}M_i}{\mathrm{d}t} = -\frac{1}{\tau}M_i + \sqrt{D^2 - \frac{\overline{N_j^n N_j^n}\left(\dfrac{\Delta t}{\tau}\right)^2}{\dfrac{3\tau}{2}(\mathrm{e}^{-2\Delta t/\tau}-1)}}\frac{\mathrm{d}W_i}{\mathrm{d}t} + N_i. \qquad (A\,6)$$

Note that f is a consistent numerical correction and has no physical meaning. Now, we are ready to show that the proposed scheme is consistent with (A 1) and (A 6) and accurately reproduces the joint second moments of velocity and position. Using Ito calculus, from (A 1) and (A 3), it follows that

$$\Delta X_i^{n+1} = M_i^{\,n}\tau(1-\mathrm{e}^{-\Delta t/\tau}) + \lim_{N\to\infty}\sum_{k=1}^{N}\xi_{k,i}\sqrt{(D^2+f)\left(\frac{\Delta t}{N}\right)}\tau(1-\mathrm{e}^{-k\Delta t/N\tau}). \qquad (A\,7)$$

Therefore,

$$\langle \Delta X_i^{n+1}\Delta X_j^{n+1}|\boldsymbol{M}^n\rangle = M_i^n M_j^n\tau^2(1-\mathrm{e}^{-\Delta t/\tau})^2 + \delta_{ij}\int_0^{\Delta t}(D^2+f)(1-\mathrm{e}^{-\Delta t/\tau})^2\mathrm{d}t. \qquad (A\,8)$$

Following the same approach for $\langle \Delta X_i^{n+1}M_j^{n+1}|\boldsymbol{M}^n\rangle$ leads to

$$\langle \Delta X_i^{n+1}M_j^{n+1}|\boldsymbol{M}^n\rangle = M_i^n M_j^n\tau(\mathrm{e}^{-\Delta t/\tau}-\mathrm{e}^{-2\Delta t/\tau}) + \delta_{ij}\int_0^{\Delta t}(D^2+f)\tau^2(\mathrm{e}^{-\Delta t/\tau}-\mathrm{e}^{-2\Delta t/\tau})\,\mathrm{d}t. \qquad (A\,9)$$

Lets consider a general form for the evolution of velocity and position. We can use independent Gaussian variables to reproduce the evolution of the joint second moments, i.e.

$$M_i^{n+1} = M_i^n \mathrm{e}^{-\Delta t/\tau} + \sqrt{\tilde{A} - \frac{C^2}{B}} \xi_{i,u} + \sqrt{\frac{C^2}{B}} \xi_{i,x} + \frac{\Delta t}{\tau} N_i^n \qquad (\mathrm{A}\,10)$$

and

$$X_i^{n+1} = X_i^n + M_i^n \tau (1 - \mathrm{e}^{-\Delta t/\tau}) + \sqrt{B} \xi_{i,x} + \frac{\Delta t^2}{2\tau} N_i^n. \qquad (\mathrm{A}\,11)$$

This is consistent with the general solutions given by (A 3) and (A 7). From above equations, the second-order statistics becomes

$$\langle \Delta X_i^{n+1} \Delta X_j^{n+1} | M^n \rangle = M_i^n M_j^n \tau^2 (1 - \mathrm{e}^{-\Delta t/\tau})^2 + \delta_{ij} B \qquad (\mathrm{A}\,12)$$

$$\langle \Delta X_i^{n+1} M_j^{n+1} | M^n \rangle = M_i^n M_j^n \tau (\mathrm{e}^{-\Delta t/\tau} - \mathrm{e}^{-2\Delta t/\tau}) + \delta_{ij} C. \qquad (\mathrm{A}\,13)$$

From the integration term in (A 8), B can be calculated as

$$B = \left(\frac{2e_s \tau^2}{3} + \frac{\tau^2 \overline{N_i^n N_i^n} \left(\dfrac{\Delta t}{\tau} \right)^2}{3(\mathrm{e}^{-2\Delta t/\tau} - 1)} \right) \left(\frac{2\Delta t}{\tau} - (1 - \mathrm{e}^{-\Delta t/\tau})(3 - \mathrm{e}^{-\Delta t/\tau}) \right), \qquad (\mathrm{A}\,14)$$

and finally C from (A 9) becomes

$$C = \left(\frac{2e_s \tau}{3} + \frac{\tau \overline{N_i^n N_i^n} \left(\dfrac{\Delta t}{\tau} \right)^2}{3(\mathrm{e}^{-2\Delta t/\tau} - 1)} \right) (1 - \mathrm{e}^{-\Delta t/\tau})^2. \qquad (\mathrm{A}\,15)$$

Appendix B. System of constitutive equations

The constitutive relations can be written as a system of linear equations, i.e.

$$\begin{pmatrix} \boldsymbol{V}_{6\times6} & \boldsymbol{W}_{6\times3} \\ \boldsymbol{X}_{3\times6} & \boldsymbol{Y}_{3\times3} \end{pmatrix} \begin{pmatrix} C_{6\times1} \\ \gamma_{3\times1} \end{pmatrix} = \begin{pmatrix} \boldsymbol{Z}_{6\times1} \\ \boldsymbol{R}_{3\times1} \end{pmatrix}, \qquad (\mathrm{B}\,1)$$

consisting of nine equations (six for P_{ij} and three for P_i) and nine unknown coefficients (six c_{ij} and three γ_i). Before we proceed, some higher order moments necessary for further derivations are presented. Moreover, for compactness, the definition

$$u_{i_1,i_2,\ldots,i_n}^{(p)} = \int_{\mathbb{R}^3} |\boldsymbol{v}'|^p v_{i_1}' v_{i_1}' \ldots v_{i_n}' f \, \mathrm{d}\boldsymbol{V} \qquad (\mathrm{B}\,2)$$

for general velocity moment is employed. For example,

$$u_{ijk}^{(0)} = \overline{u_i' u_j' u_k'}, \qquad (\mathrm{B}\,3)$$

$$u_i^{(2)} = \overline{u_i' u_j' u_j'}, \qquad (\mathrm{B}\,4)$$

$$u^{(4)} = \overline{u_i' u_i' u_j' u_j'}, \qquad (\mathrm{B}\,5)$$

$$u_{ij}^{(2)} = \overline{u_i' u_j' u_l' u_l'} \qquad (\mathrm{B}\,6)$$

$$u_{ij}^{(4)} = \overline{u_i' u_j' u_l' u_l' u_k' u_k'} \qquad (\mathrm{B}\,7)$$

contribute to the blocks in the system (B 1). Now, based on the constitutive relations, i.e. (2.21) and (2.22), we present the blocks in the linear system (B 1), i.e. the upper right matrix block

$$
\boldsymbol{W}_{6\times3} = \begin{pmatrix}
2u_1^{(2)} & 0 & 0 \\
u_2^{(2)} & u_1^{(2)} & 0 \\
u_3^{(2)} & 0 & u_1^{(2)} \\
0 & 2u_2^{(2)} & 0 \\
0 & u_3^{(2)} & u_2^{(2)} \\
0 & 0 & 2u_3^{(2)}
\end{pmatrix}, \tag{B 8}
$$

the upper left matrix block

$$
\boldsymbol{V}_{6\times6} = \begin{pmatrix}
2u_{11}^{(2)} & 2u_{12}^{(2)} & 2u_{13}^{(2)} & 0 & 0 & 0 \\
u_{12}^{(2)} & u_{22}^{(2)}+u_{11}^{(2)} & u_{23}^{(2)} & u_{12}^{(2)} & u_{13}^{(2)} & 0 \\
u_{13}^{(2)} & u_{23}^{(2)} & u_{33}^{(2)}+u_{11}^{(2)} & 0 & u_{12}^{(2)} & u_{13}^{(2)} \\
0 & 2u_{12}^{(2)} & 0 & 2u_{22}^{(2)} & 2u_{23}^{(2)} & 0 \\
0 & u_{13}^{(2)} & u_{12}^{(2)} & u_{23}^{(2)} & u_{33}^{(2)}+u_{22}^{(2)} & u_{23}^{(2)} \\
0 & 0 & 2u_{13}^{(2)} & 0 & 2u_{23}^{(2)} & 2u_{33}^{(2)}
\end{pmatrix}, \tag{B 9}
$$

the transpose of the lower left matrix block

$$
\boldsymbol{X}_{3\times6}^{\mathrm{T}} = 2 \begin{pmatrix}
u_{111}^{(2)}-u_{11}^{(0)}u_1^{(2)} & 2(u_{112}^{(2)}-u_{11}^{(0)}u_2^{(2)}) & u_{113}^{(2)}-u_{13}^{(0)}u_1^{(2)} \\
2(u_{112}^{(2)}-u_{11}^{(0)}u_2^{(2)}) & 2(u_{122}^{(2)}-u_{12}^{(0)}u_2^{(2)}) & 2(u_{123}^{(2)}-u_{23}^{(0)}u_1^{(2)}) \\
2(u_{113}^{(2)}-u_{11}^{(0)}u_3^{(2)}) & 2(u_{123}^{(2)}-u_{12}^{(0)}u_3^{(2)}) & 2(u_{133}^{(2)}-u_{13}^{(0)}u_2^{(2)}) \\
u_{122}^{(2)}-u_{12}^{(0)}u_2^{(2)} & u_{222}^{(2)}-u_{22}^{(0)}u_2^{(2)} & u_{233}^{(2)}-u_{23}^{(0)}u_2^{(2)} \\
2(u_{123}^{(2)}-u_{12}^{(0)}u_3^{(2)}) & 2(u_{223}^{(2)}-u_{22}^{(0)}u_3^{(2)}) & 2(u_{233}^{(2)}-u_{22}^{(0)}u_3^{(2)}) \\
u_{133}^{(2)}-u_{13}^{(0)}u_3^{(2)} & u_{233}^{(2)}-u_{23}^{(0)}u_3^{(2)} & u_{333}^{(2)}-u_{33}^{(0)}u_3^{(2)}
\end{pmatrix}
$$
$$
+ \begin{pmatrix}
u_1^{(4)}-u_1^{(2)}u^{(2)} & 0 & 0 \\
u_2^{(4)}-u_2^{(2)}u^{(2)} & u_1^{(4)}-u_1^{(2)}u^{(2)} & 0 \\
u_3^{(4)}-u_3^{(2)}u^{(2)} & 0 & u_1^{(4)}-u_1^{(2)}u^{(2)} \\
0 & u_2^{(4)}-u_2^{(2)}u^{(2)} & 0 \\
0 & u_3^{(4)}-u_3^{(2)}u^{(2)} & u_2^{(4)}-u_2^{(2)}u^{(2)} \\
0 & 0 & u_3^{(4)}-u_3^{(2)}u^{(2)}
\end{pmatrix}, \tag{B 10}
$$

the lower right matrix block

$$\mathbf{Y}_{3\times3} = -2u^{(2)} \begin{pmatrix} u_{11}^{(0)} & u_{12}^{(0)} & u_{13}^{(0)} \\ u_{12}^{(0)} & u_{22}^{(0)} & u_{23}^{(0)} \\ u_{13}^{(0)} & u_{23}^{(0)} & u_{33}^{(0)} \end{pmatrix} + 2 \begin{pmatrix} u_{11}^{(2)} & u_{12}^{(2)} & u_{13}^{(2)} \\ u_{12}^{(2)} & u_{22}^{(2)} & u_{23}^{(2)} \\ u_{13}^{(2)} & u_{23}^{(2)} & u_{33}^{(2)} \end{pmatrix}$$
$$+ (u^{(4)} - (u^{(2)})^2) I_{3\times3}, \tag{B 11}$$

the upper right-hand side vector

$$\mathbf{Z}_{6\times1} = -2\Lambda \begin{pmatrix} u_{11}^{(2)} \\ u_{12}^{(2)} \\ u_{13}^{(2)} \\ u_{22}^{(2)} \\ u_{23}^{(2)} \\ u_{33}^{(2)} \end{pmatrix} \tag{B 12}$$

and the lower right-hand side vector

$$\mathbf{R}_{3\times1} = (-2Pr + 3) \begin{pmatrix} u_1^{(2)} \\ u_2^{(2)} \\ u_3^{(2)} \end{pmatrix}$$
$$+ \Lambda \begin{pmatrix} -3u_1^{(4)} + u^{(2)}u_1^{(2)} + 2\left(u_{11}^{(0)}u_1^{(2)} + u_{12}^{(0)}u_2^{(2)} + u_{13}^{(0)}u_3^{(2)}\right) \\ -3u_2^{(4)} + u^{(2)}u_2^{(2)} + 2\left(u_{12}^{(0)}u_1^{(2)} + u_{22}^{(0)}u_2^{(2)} + u_{23}^{(0)}u_3^{(2)}\right) \\ -3u_3^{(4)} + u^{(2)}u_3^{(2)} + 2\left(u_{13}^{(0)}u_1^{(2)} + u_{23}^{(0)}u_2^{(2)} + u_{33}^{(0)}u_3^{(2)}\right) \end{pmatrix}. \tag{B 13}$$

REFERENCES

AGARWAL, R. K., YUN, K. & BALAKRISHNAN, R. 2001 Beyond Navier–Stokes: Burnett equations for flows in the continuum-transition regime. *Phys. Fluids* **13**, 3061–3085.

BESKOK, A. & KARNIADAKIS, G. E. 1999 A model for flows in channels and ducts at micro and nano scales. *Microscale Thermophys. Engng* **3**, 43–77.

BHATNAGAR, P. L., GROSS, E. P. & KROOK, M. 1954 A model for collision processes in gases. I. Small amplitude processes in charged and neutral one-component systems. *Phys. Rev.* **94**, 511–525.

BIRD, G. 1994 *Molecular Gas Dynamics and the Direct Simulation of Gas Flows.* Calerndon.

CERCIGNANI, C. 1964 Higher order slip according to the linearized Boltzmann equation. *Res. Rep.* AS-64-19. University of California, Berkeley, Institute of Engineering.

CERCIGNANI, C. 1988 *The Boltzmann Equation and Its Applications.* Springer-Verlag.

CHANDRASEKHAR, S. 1943 Stochastic problems in physics and astronomy. *Rev. Mod. Phys.* **15**, 1–89.

DAGUM, L. 1991 Three-Dimensional Direct Particle Simulation on the Connection Machine. *AIAA Paper* No. 91-1365, Reston, VA.

DONG, W. 1956 From stochastic processes to the hydrodynamic equations. *Res. Rep.* UCRL-3353. University of California.

GARDINER, C. W. 1985 *Handbook of Stochastic Methods.* Springer-Verlag.

HADJICONSTANTINOU, N. G. 2003 Comment on Cercignani's second-order slip coefficient. *Phys. Fluids* **15**, 2352–2354.

HEINZ, S. 2004 Molecular to fluid dynamics: the consequences of stochastic molecular motion. *Phys. Rev. E* **70**, 036308.

HOLWAY, L. H. 1966 New statistical models for kinetic theory: methods of construction. *Phys. Fluids* **9**, 1658–1673.

JENNY, P., POPE, S. B., MURADOGLU, M. & CAUGHEY, D. 2001 A hybrid algorithm for the joint pdf equation of turbulent reactive flows. *J. Comput. Phys.* **166**, 218–252.

JENNY, P., TORRILHON, M. & HEINZ, S. 2010 A solution algorithm for the fluid dynamics equations based on a stochastic model for molecular motion. *J. Comput. Phys.* **229**, 1077–1098.

LEBOWITZ, J. L., FRISCH, H. L. & HELFAND, E. 1960 Nonequilibrium distribution functions in a fluid. *Phys. Fluids* **3**, 325–338.

OHWADA, T., SONE, Y. & AOKI, K. 1989 Numerical analysis of the Poiseuille flow and thermal transpiration flows between two parallel plates on the basis of the linearized Boltzmann equation for hard-sphere molecules. *Phys. Fluids* **1**, 2042–2049.

PAWULA, R. F. 1967 Approximation of the linear Boltzmann equation by the Fokker–Planck equation. *Phys. Rev.* **162**, 186–188.

RISKEN, H. 1989 *The Fokker–Planck Equation, Methods of Solution and Applications.* Springer-Verlag.

SHAKHOV, E. M. 1968 Generalization of the Krook kinetic relaxation equation. *Fluid Dynamics* **3**, 142–145.

SHARIPOV, F. 2002 Application of the Cercignani–Lampis scattering kernel to calculations of rarefied gas flows. I. Plane flow between two parallel plates. *Eur. J. Mech. (B/Fluids)* **21**, 113–123.

SHARIPOV, F. & SELEZNEV, V. 1998 Data on internal Rarefied gas flows. *J. Phys. Chem.* **27**, 657–706.

SHIINO, M. 1987 Dynamical behavior of stochastic systems of infinitely many coupled nonlinear oscillators exhibiting phase transitions of mean-field type: H theorem on asymptotic approach to equilibrium and critical slowing down of order-parameter fluctuations. *Phys. Rev. E* **36**, 2393–2412.

SPRINGER, G. S. 1971 Heat transfer in rarefied gases. *Adv. Heat Transfer* **7**, 163–218.

STRUCHTRUP, H. 2005 *Macroscopic Transport Equations for Rarefied Gas Flows.* Springer.

TAHERI, P., TORRILHON, M. & STRUCHTRUP, H. 2009 Couette and Poiseuille microflows: Analytical solutions for regularized 13-moment equations. *Phys. Fluids* **21**, 017102.

TORRILHON, M. & STRUCHTRUP, H. 2004 Regularized 13-moment equations: shock structure calculations and comparison to Burnett models. *J. Fluid Mech.* **513**, 171–198.

TORRILHON, M. & STRUCHTRUP, H. 2008 Boundary conditions for regularized 13-moment-equations for microchannel-flows. *J. Comput. Phys.* **227**, 1982–2011.

TORRILHON, M. & STRUCHTRUP, H. 2009 Modeling micro mass and heat transfer for gases using extended continuum equations. *J. Heat Transfer* **131**, 033103.

TRUESDELL, C. & MUNCASTER, R. G. 1980 *Fundamentals of Maxwell's Kinetic Theory of a Simple Monatomic Gas.* Academic.

XU, K. 2003 Super-Burnett solutions of Poiseuille flow. *Phys. Fluids* **15**, 2077.

XU, K. 2004 Microchannel flow in the slip regime: gas-kinetic BGK–Burnett solutions. *J. Fluid Mech.* **513**, 87–110.

YANO, R., SUZUKI, K. & KURODA, H. 2009 Analytical and numerical study on the nonequilibrium relaxation by the simplified Fokker–Planck equation. *Phys. Fluids* **21**, 047104.

ZHENG, Y., GARCIA, A. L. & ALDER, B. J. 2002 A comparison of kinetic theory and hydrodynamics for Poiseuille flow. *J. Stat. Phys.* **109**, 495–505.

ZHENG, Y., REESE, J. M. & STRUCHTRUP, H. 2006 Comparing macroscopic continuum models for rarefied gas dynamics: A new test method. *J. Comput. Phys.* **218**, 748–769.